ORIGINAL PAPER

Monitoring mean of INAR(1) process with discrete mixture exponential innovations

M. R. Irshad[1] · Muhammed Ahammed[1] · R. Maya[2]

Abstract

This paper presents a discrete counterpart of the mixture exponential distribution, namely discrete mixture exponential distribution, by utilizing the survival discretization method. The moment generating function and associated moment measures are discussed. The distribution's hazard rate function can assume increasing or decreasing forms, making it adaptable for diverse fields requiring count data modeling. The paper delves into two parameter estimation methods and evaluates their performance through a Monte Carlo simulation study. The applicability of this distribution extends to time series analysis, particularly within the framework of the first-order integer-valued autoregressive process. Consequently, an INAR(1) process with discrete mixture exponential innovations is proposed, outlining its fundamental properties, and the performance of conditional maximum likelihood and conditional least squares estimation methods is evaluated through a simulation study. Real data analysis showcases the proposed model's superior performance compared to alternative models. Additionally, the paper explores quality control applications, addressing serial dependence challenges in count data encountered in production and market management. As a result, the INAR(1)DME process is employed to explore control charts for monitoring autocorrelated count data. The performance of two distinct control charts, the cumulative sum chart and the exponentially weighted moving average chart, are evaluated for their effectiveness in detecting shifts in the process mean across various designs. A bivariate Markov chain approach is used to estimate the average run length and their deviations for these charts, providing valuable insights for practical implementation. The nature of design parameters to improve the robustness of process monitoring under the considered charts is examined through a simulation study. The practical superiority of the proposed charts is demonstrated through effective modeling with real data, surpassing competing models.

✉ M. R. Irshad
  irshadmr@cusat.ac.in

[1] Department of Statistics, Cochin University of Science and Technology, Cochin, Kerala 682 022, India

[2] Department of Statistics, University College, Thiruvananthapuram, Kerala 695 034, India

🙋 Springer

1 Introduction

Statistical quality control involves applying statistical methods to monitor and control processes, with the primary objective of ensuring consistency and compliance with predefined criteria. This underscores the critical importance of count data modeling in ensuring the accuracy and effectiveness of quality control measures. The serial dependence inherent in count data enables the effective use of integer-valued autoregressive time series models. Consequently, there is a growing recognition of the necessity for more flexible discrete models.

Time series models serve as indispensable tools for capturing distinct data features, especially when dealing with count data over time. The first-order integer-valued autoregressive (INAR(1)) process is a significant statistical model for studying autocorrelated count data, excelling in accurately representing counts when compared to Poisson and negative binomial models. Consequently, Al-Osh and Alzaid (1987) introduced the INAR(1) process with binomial thinning having Poisson marginals. Subsequently, other variations, such as the INAR(1) process with Poisson-transmuted exponential innovations proposed by Altun and Khan (2022), INAR(1) process with Poisson-extended exponential innovations presented by Maya et al. (2022), and INAR(1) process with new discrete Bilal innovations discussed by Ahsan-ul Haq et al. (2023), have emerged. Researchers are exploring these INAR(1) models to enhance their ability to fit real datasets optimally. This diverse collection of INAR(1) models has garnered substantial interest among researchers, undergoing in-depth exploration and contributing to the evolving landscape of time series modeling, particularly in fields like quality control.

Statistical quality control primarily focuses on count data, and the introduction of control charts has revolutionized this field, making them the primary method for process monitoring. Control charts are designed to maintain process stability and swiftly detect parameter shifts, classifying a process as "in control" if it adheres to a specified model. Consequently, efficient monitoring is essential to identify shifts in the mean promptly. The cumulative sum (CUSUM) and exponentially weighted moving average (EWMA) control charts are recognized for their ability to retain information over time and detect these changes. The frequently used conventional control charts often assume independent observations, a premise that may not consistently align with real-world scenarios. This necessitates the utilization of control charts in integer-valued time series models. As a result, Weiß and Testik (2011) proposed a CUSUM chart for monitoring the mean of the INAR(1) process with Poisson marginals. Some of the notable works include Li et al. (2022), Kim and Lee (2017) and Rakitzis et al. (2017). To enhance monitoring capabilities, EWMA charts have been introduced and compared with CUSUM charts. Following the CUSUM chart, Weiß (2011) discussed the corresponding EWMA chart. Some other works include Li et al. (2016, 2019) and Zhang et al. (2014).

Building on this foundation, our study delves into assessing the effectiveness of control charts in monitoring an INAR(1) process. Within this context, the

associated discrete distributions are crucial in modeling the data. Although count data modeling has traditionally relied on Poisson and negative binomial distributions, the widespread occurrence of over-dispersion and notable skewness or kurtosis in real-world datasets has emphasized the necessity to create new models. Hence, we introduce a new discrete distribution and its associated INAR(1) process, incorporating it as innovations. Researchers have responded by introducing innovative discrete distributions through various methodologies. Here, we utilize survival discretization technique, and for a random variable (rv) X having a survival function $\bar{F}(x) = P(X > x)$, the corresponding probability mass function (pmf) is given by,

$$P(X = x) = \bar{F}(x) - \bar{F}(x + 1), \ x = 0, 1, 2, 3, \dots . \tag{1.1}$$

This method retains the shape of the hazard rate function (hrf) of the base model. Some of the works based on the above model include Krishna and Pundir (2009), El-Morshedy et al. (2020) and Altun et al. (2022).

Motivated by the aforementioned works, this study introduces a novel discrete mixture exponential (DME) distribution by utilizing survival discretization technique to the mixture exponential (ME) distribution proposed by Mirhossaini and Dolati (2008). The distribution's statistical characteristics are examined, and the performance of parameter estimation approaches is assessed through a simulation study. The superior performance of the DME distribution in real data analysis allows us to explore the INAR(1) process with DME distributed innovation, denoted as the INAR(1)DME process. The superior performance of the INAR(1) DME process in real data analysis further enables us to utilize it in the field of quality control

In the context of quality control, to monitor the mean of the INAR(1)DME process, CUSUM and EWMA control charts are developed, and their statistical design and performance in detecting increasing shifts in process mean levels are investigated. The analysis encompasses the evaluation of control chart properties, particularly their average run length (ARL), which indicates their sensitivity in detecting mean changes within the process. A comparative assessment of both monitoring approaches is also undertaken, providing insights into their performance. The effectiveness of the control chart under the INAR(1)DME process in detecting shifts in the process mean is assessed by utilizing real data.

The paper is structured as follows: Sect. 2 provides an overview of the construction and characteristics of the DME distribution. Section 3 introduces the associated statistical properties, including the moment generating function (mgf), moments, skewness, and kurtosis. Section 4 delves into the discussion of parameter estimation methods and assessing their performance using a Monte Carlo simulation study. Section 5 evaluates the performance of the proposed distribution using a real data set. Section 6 introduces the INAR(1) process with DME innovations and discusses its properties, including estimation, simulation, and real data analysis. Section 7 focuses on the statistical process control procedure for INAR(1)DME processes, utilizing the CUSUM and EWMA approaches to detect mean increases, accompanied by numerical simulation and real data analysis. The study is concluded in Sect. 8.

2 The discrete mixture exponential distribution

Let X be a rv following the ME distribution. The probability density function and cumulative distribution function (cdf) of the ME distribution are given by,

$$g(x;\alpha,\theta) = \theta e^{-\theta x}\left\{1 + \alpha\left(2e^{-\theta x} - 1\right)\right\}, \quad x > 0,$$

and

$$G(x;\alpha,\theta) = \left(1 - e^{-\theta x}\right)\left(1 + \alpha e^{-\theta x}\right), \quad x > 0, \tag{2.1}$$

where $\theta > 0$, $-1 \leq \alpha \leq 1$.

Applying (1.1) to (2.1), along with the reparameterization $\lambda = e^{-\theta}$, yields the DME distribution, as outlined in the following proposition.

Proposition 2.1 *Let $X \sim \text{DME}(\alpha, \lambda)$, then the pmf is given by,*

$$P(X = x) = \lambda^x (1 - \lambda)(1 - \alpha) + \alpha \lambda^{2x} (1 - \lambda^2), \ x = 0, 1, 2, ..., \tag{2.2}$$

where $0 < \lambda < 1$ and $-1 \leq \alpha \leq 1$.

The corresponding cdf is given by,

$$F(x) = \left(1 - \lambda^{(1+x)}\right)\left(1 + \alpha\lambda^{(1+x)}\right).$$

The pmf of the DME distribution always decreases for $-0.3 < \alpha < 1$ since,

$$p'(x) = (1 - \alpha)(1 - \lambda)\lambda^x \log(\lambda) + 2\alpha \lambda^{2x}(1 - \lambda^2)\log(\lambda) < 0.$$

Figure 1 displays the pmf plots of the DME distribution. It can be seen that the DME distribution is rightly skewed and unimodal.

3 Statistical properties

This section discusses the DME distribution's hrf, mgf, moments, skewness, and kurtosis. The hrf of the DME distribution is obtained as,

$$h(x) = \frac{(1 - \lambda)(1 + \alpha(\lambda^x + \lambda^{(1+x)} - 1))}{\lambda - \alpha\lambda + \alpha\lambda^{(2+x)}}.$$

Figure 2 showcases the DME distribution's hrf, illustrating its ability to exhibit increasing ($-1 \leq \alpha < 0$), decreasing ($0 < \alpha < 1$) and constant ($\alpha = 0$) behaviors.
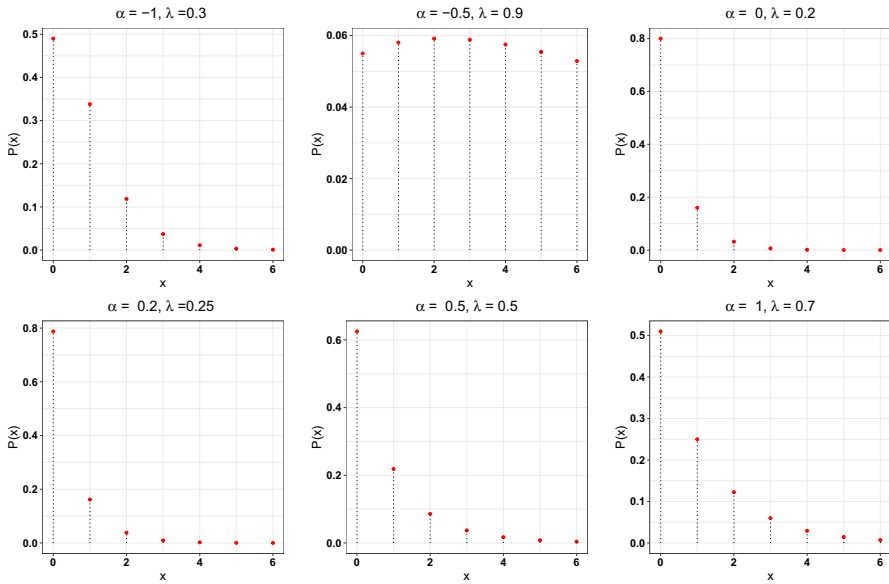
The mgf of the DME distribution is given by,

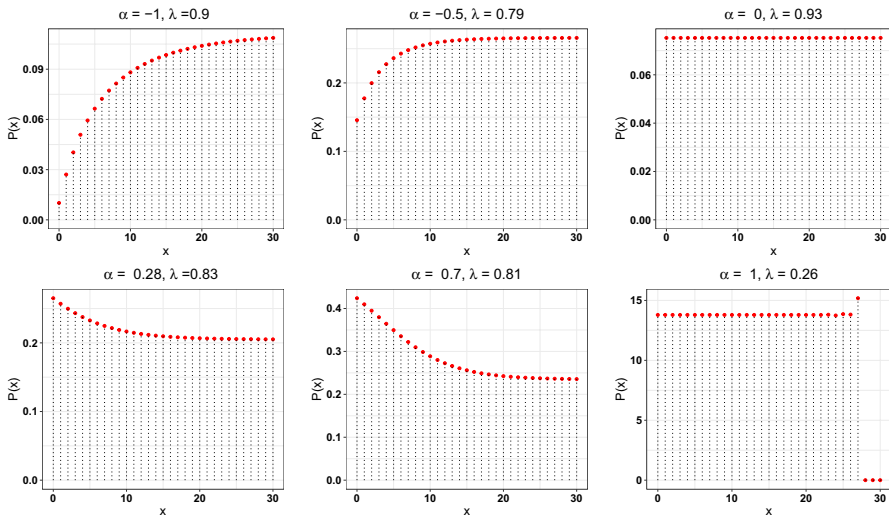**Fig. 1** Pmfs of the DME distribution for different parameter values

Fig. 2 Hazard rate function of the DME distribution for different parameter values

$$M_X(t) = \sum_{x=0}^{\infty} e^{tx} \{\lambda^x(1-\lambda)(1-\alpha) + \alpha\lambda^{2x}(1-\lambda^2)\}$$

$$= \frac{(1-\lambda)(1-\alpha)}{1-\lambda e^t} + \frac{\alpha(1-\lambda^2)}{1-\lambda^2 e^t}$$

$$= \frac{(1-\lambda)((e^t-1)\alpha\lambda + e^t\lambda^2 - 1)}{((1-e^t\lambda)(e^t\lambda^2 - 1))}, \quad \lambda e^t < 1.$$

The *r*th moment about the origin of *X* is given by,

$$\mu'_r = \sum_{x=0}^{\infty} x^r \lambda^x(1-\lambda)(1-\alpha) + \alpha\lambda^{2x}(1-\lambda^2), \quad r = 1, 2, 3, ..$$

Then, the mean and variance of the DME distribution are given by,

$$E(X) = \frac{\lambda(1-\alpha+\lambda)}{(1-\lambda^2)} \text{ and } Var(X) = \frac{\lambda((1+\lambda)^2 - \alpha^2\lambda - \alpha(1+\lambda^2))}{(1-\lambda^2)^2}. \quad (3.1)$$

Using (3.1), the dispersion index (DI) of the DME distribution, which quantifies variability, is given by,

$$DI(X) = \frac{Var(X)}{E(X)} = \frac{\alpha^2\lambda - (1+\lambda)^2 + \alpha(1+\lambda^2)}{(\lambda-1)(1+\lambda)(1-\alpha+\lambda)}.$$

The shape and characteristics of the DME distribution are analyzed using the moment measures of skewness and kurtosis, which are given by,

$$S(X) = \frac{\left[E(X-E(X))^3\right]^2}{[Var(X)]^3}$$

$$= \frac{((1+\lambda)^3(-1-3\lambda+4\lambda^2) + \alpha^2\lambda(1+6\lambda+11\lambda^2) + \alpha(1+4\lambda+2\lambda^2-16\lambda^3-9\lambda^4))^2}{\lambda((1+\lambda)^2 - \alpha^2\lambda - \alpha(1+\lambda^2))^3},$$

$$K(X) = \frac{E(X-E(X))^4}{[Var(X)]^2}$$

$$= \frac{(1+\lambda)^4(1+7\lambda+\lambda^2) - 3\alpha^4\lambda^3 - 6\alpha^3(\lambda^2+\lambda^4) - 2\alpha^2\lambda(2+3\lambda+14\lambda^2+3\lambda^3+2\lambda^4)}{\lambda(\alpha^2\lambda - (1+\lambda)^2 + \alpha(1+\lambda^2))^2}$$

$$- \frac{\alpha(1+6\lambda+23\lambda^2+12\lambda^3+23\lambda^4+6\lambda^5+\lambda^6)}{\lambda(\alpha^2\lambda - (1+\lambda)^2 + \alpha(1+\lambda^2))^2}.$$

See "Appendix" for more details.

From the 3D plot of DI given in Fig. 3, it is clear that DI is greater than 1. The 3D plots in Fig. 4 illustrate the graphical representation of skewness and kurtosis, indicating the right-skewed leptokurtic behavior of the DME distribution. Table 1 illustrates the variation in mean, variance, DI, skewness, and kurtosis with respect to the values of α and λ. The mean, variance and DI consistently increase, while skewness

Fig. 3 DI of the DME distribution for different parameter values

(a)

(b)
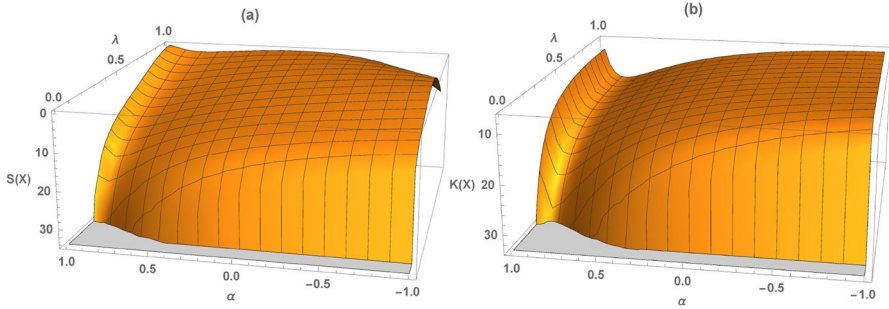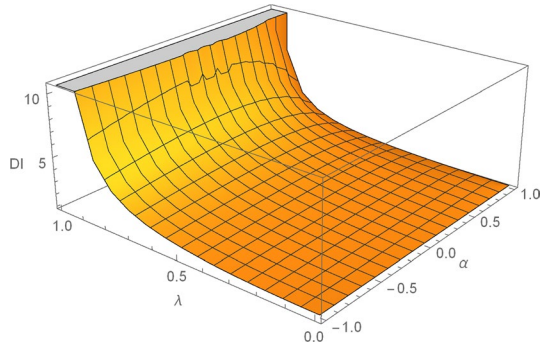
Fig. 4 Skewness (**a**) and kurtosis (**b**) of the DME distribution for different parameter values

and kurtosis decrease with the rise in λ for a fixed $\alpha \in [-1, 1]$ and $\alpha \in (-0.3, 1]$, respectively.

4 Estimation

This section discusses the maximum likelihood (ML) and least squares (LS) parameter estimation for the DME distribution.

4.1 Maximum likelihood estimation

Let $x = (x_1, x_2, ..., x_n)$ be a sample of size n from the DME distribution. Then, the log-likelihood function is given by,

$$\log L(\alpha, \lambda) = \sum_{i=1}^{n} \log\{\lambda^{x_i}(1 - \lambda)(1 - \alpha) + \alpha\lambda^{2x_i}(1 - \lambda^2)\}. \tag{4.1}$$

Since $\frac{\partial \log L(\alpha,\lambda)}{\partial \alpha} = 0$ and $\frac{\partial \log L(\alpha,\lambda)}{\partial \lambda} = 0$ failed to give explicit solutions, the maximum likelihood estimates (MLEs) $\hat{\alpha}$ and $\hat{\lambda}$ of α and λ are obtained by direct maximization

Table 1 The mean, variance, DI, skewness and kurtosis of the DME distribution

$\alpha = -1$						$\alpha = -0.7$					
λ	$E(X)$	$Var(X)$	DI	$S(X)$	$K(X)$	λ	$E(X)$	$Var(X)$	DI	$S(X)$	$K(X)$
0.2	0.46	0.49	1.08	5.77	6.99	0.2	0.40	0.45	1.13	6.69	7.93
0.5	1.67	2.67	1.60	0.51	6.88	0.5	1.47	2.56	1.75	1.38	7.22
0.7	3.71	9.90	2.67	0.63	7.01	0.7	3.29	9.66	2.93	0.00	7.22
0.8	6.22	25.19	4.05	2.55	7.05	0.8	5.56	24.67	4.44	0.42	7.22
0.9	13.74	112.69	8.20	5.81	7.07	0.9	12.32	110.59	8.98	1.70	7.23

$\alpha = -0.4$						$\alpha = 0$					
λ	$E(X)$	$Var(X)$	DI	$S(X)$	$K(X)$	λ	$E(X)$	$Var(X)$	DI	$S(X)$	$K(X)$
0.2	0.33	0.40	1.19	7.91	9.28	0.2	0.25	0.31	1.25	10.37	12.20
0.5	1.27	2.37	1.87	2.52	7.89	0.5	1.00	2.00	2.00	4.50	9.50
0.7	2.88	9.08	3.15	0.40	7.75	0.7	2.33	7.78	3.33	1.86	9.13
0.8	4.89	23.26	4.76	0.01	7.72	0.8	4.00	20.00	5.00	0.88	9.05
0.9	10.89	104.46	9.59	0.19	7.71	0.9	9.00	90.00	10.00	0.24	9.01

$\alpha = 0.1$						$\alpha = 0.4$					
λ	$E(X)$	$Var(X)$	DI	$S(X)$	$K(X)$	λ	$E(X)$	$Var(X)$	DI	$S(X)$	$K(X)$
0.2	0.23	0.29	1.26	11.23	13.26	0.2	0.17	0.22	1.29	14.96	17.97
0.5	0.93	1.88	2.02	5.11	10.09	0.5	0.73	1.48	2.02	7.39	12.59
0.7	2.20	7.36	3.35	2.36	9.65	0.7	1.78	5.87	3.29	4.25	11.81
0.8	3.78	18.94	5.01	1.28	9.55	0.8	3.11	15.16	4.87	2.85	11.65
0.9	8.53	85.26	10.00	0.48	9.50	0.9	7.11	68.36	9.62	1.62	11.57

$\alpha = 0.7$						$\alpha = 1$					
λ	$E(X)$	$Var(X)$	DI	$S(X)$	$K(X)$	λ	$E(X)$	$Var(X)$	DI	$S(X)$	$K(X)$
0.2	0.10	0.13	1.28	22.18	27.39	0.2	0.04	0.04	1.04	31.00	32.04
0.5	0.33	0.54	1.62	12.82	18.22	0.5	0.33	0.44	1.33	9.00	11.25
0.7	1.37	4.05	2.95	6.64	15.16	0.7	0.96	1.88	1.96	4.65	9.53
0.8	2.44	10.49	4.29	4.80	14.85	0.8	1.78	4.94	2.78	2.57	9.20
0.9	5.68	47.42	8.34	3.05	14.70	0.9	4.26	22.44	5.26	0.80	9.04

of (4.1) using numerical methods. To this end, one can use the `optim` function in R software.

The observed Fisher information matrix of $\hat{\alpha}$ and $\hat{\lambda}$ is given by,

$$\hat{J}_n = - \left[\begin{matrix} \frac{\partial^2 \log L(\alpha,\lambda)}{\partial \alpha^2} & \frac{\partial^2 \log L(\alpha,\lambda)}{\partial \alpha \partial \lambda} \\ \frac{\partial^2 \log L(\alpha,\lambda)}{\partial \lambda \partial \alpha} & \frac{\partial^2 \log L(\alpha,\lambda)}{\partial \lambda^2} \end{matrix} \right] \Bigg|_{(\alpha,\lambda)=(\hat{\alpha},\hat{\lambda})}$$

Hence, the variance-covariance matrix is obtained as

$$\Sigma = \hat{J}_n^{-1}.$$

4.2 Least squares estimation

Let $x_{i:n}$ be the ith order statistic of the sample $x = (x_1, x_2, .., x_n)$. The LS estimates (LSEs) of the parameters are obtained by minimizing the following equation:

$$LSE(\alpha, \lambda) = \sum_{i=1}^{n} \left[\{(1 - \lambda^{(1+x_{i:n})})(1 + \alpha\lambda^{(1+x_{i:n})})\} - \frac{i}{n+1} \right]^2.$$

To this end, one can use the `optim` function in R software.

4.3 Simulation

The performance of the estimation methods is assessed through a simulation study. The simulation is conducted with $N = 1000$ replications for sample sizes n of 100, 200, 300, 400, and 500, encompassing various parameter values. The following quantities are computed.

1. Average bias (Bias), Bias($\hat{a}$)=$\frac{1}{N} \sum_{i=1}^{N}(\hat{a}_i - a)$, where $\hat{a}_i$ is the ith estimate of the parameter a, $a \in \{\alpha, \lambda\}$, for $i = 1, 2, \ldots, N$.
2. Root mean square error (RMSE), RMSE($\hat{a}$) = $\sqrt{\frac{1}{N} \sum_{i=1}^{N}(\hat{a}_i - a)^2}$.

Table 2 lists the Bias and RMSE for the MLEs and LSEs of the parameters α and λ. As n increases, both Bias and RMSE decrease for the ML and LS methods. Additionally, a significant decrease in both Bias and RMSE is observed when comparing the ML method to the LS. Thus, ML estimation performs very well and is appropriate for small and large sample sizes.

5 Data analysis

The corn-borer data comprises 120 observations of European corn-borer larvae (Pyrausta) numbers in the field (Bodhisuwan and Sangpoom 2016), is considered to to evaluate how well the DME distribution fits the data. The Poisson distribution, the discrete Burr (DB) distribution (Krishna and Pundir 2009), the discrete Gumbel (DG) distribution (Chakraborty and Chakravarty 2014), the discrete log-logistic (DLL) distribution (Para and Jan 2016), the discrete Bilal (DBL) distribution (Altun

Table 2 Simulation results of the DME distribution

n	MLE						LSE					
	α			λ			α			λ		
	Estimate	Bias	RMSE	Estimate	Bias	RMSE	Estimate	Bias	RMSE	Estimate	Bias	RMSE
α = −1, λ = 0.9												
100	−0.966	0.034	0.066	0.901	0.006	0.007	−0.972	0.028	0.063	0.906	0.007	0.009
200	−0.975	0.025	0.049	0.902	0.004	0.005	−0.985	0.015	0.037	0.906	0.006	0.007
300	−0.983	0.017	0.033	0.902	0.003	0.004	−0.993	0.007	0.021	0.905	0.006	0.006
400	−0.984	0.016	0.031	0.901	0.003	0.003	−0.995	0.005	0.016	0.905	0.005	0.006
500	−0.985	0.015	0.027	0.902	0.002	0.003	−0.997	0.003	0.012	0.905	0.005	0.006
α = −0.6, λ = 0.9												
100	−0.622	0.142	0.187	0.899	0.008	0.01	−0.72	0.178	0.214	0.9	0.008	0.01
200	−0.617	0.094	0.134	0.9	0.005	0.007	−0.737	0.161	0.187	0.9	0.005	0.007
300	−0.626	0.076	0.103	0.9	0.004	0.005	−0.755	0.164	0.183	0.899	0.004	0.005
400	−0.622	0.062	0.083	0.9	0.003	0.004	−0.751	0.155	0.17	0.9	0.003	0.004
500	−0.618	0.054	0.074	0.9	0.003	0.004	−0.749	0.153	0.166	0.899	0.003	0.004
α = 0.25, λ = 0.73												
100	0.188	0.295	0.357	0.722	0.043	0.053	0.491	0.81	0.53	0.64	0.09	0.098
200	0.236	0.248	0.304	0.727	0.035	0.043	0.423	0.63	0.69	0.635	0.095	0.099
300	0.266	0.225	0.28	0.732	0.032	0.04	0.42	0.73	0.77	0.634	0.096	0.099
400	0.264	0.193	0.245	0.732	0.027	0.035	0.416	0.7	0.73	0.634	0.096	0.097
500	0.267	0.177	0.229	0.732	0.026	0.033	0.415	0.74	0.77	0.634	0.096	0.098
α = 0.5, λ = 0.8												
100	0.347	0.301	0.388	0.779	0.04	0.051	0.81	0.84	0.78	0.698	0.109	0.115
200	0.41	0.249	0.308	0.788	0.032	0.04	0.7	0.88	0.76	0.685	0.116	0.119
300	0.435	0.227	0.28	0.791	0.029	0.036	0.713	0.85	0.72	0.683	0.117	0.119

Table 2 (continued)

n	MLE						LSE					
	α			λ			α			λ		
	Estimate	Bias	RMSE	Estimate	Bias	RMSE	Estimate	Bias	RMSE	Estimate	Bias	RMSE
400	0.45	0.214	0.261	0.793	0.026	0.032	0.718	0.78	0.69	0.683	0.117	0.118
500	0.456	0.187	0.229	0.794	0.024	0.029	0.716	0.76	0.68	0.683	0.117	0.118

et al. 2022), the discrete Pareto (DPR) distribution (Krishna and Pundir 2009), and the discrete Rayleigh (DR) distribution (Roy 2004), are chosen for comparison.

The unknown parameters are obtained using the ML method, along with the standard error (SE) and 95% confidence interval (CI) for the considered models. Model performance is assessed using some widely accepted information criteria and goodness-of-fit statistics. Smaller values of the Akaike information criterion (AIC) and Bayesian information criterion (BIC), as well as larger log-likelihood (logL) values, indicate the adequacy of the model. Furthermore, the goodness-of-fit for each fitted distribution is assessed using the chi-square test, where a small χ^2 value and a large p-value indicate a good fit.

Table 3 makes it abundantly clear that the DME distribution is the best of the competitive models under consideration because it has the lowest AIC and BIC, the highest logL, and p-value, respectively.

The observed and expected frequencies of corn-borer data under various distributions are displayed in Fig. 5. The expected frequencies align more closely with the theoretical values under the DME distribution than the other considered distributions. Hence, the DME distribution performs better than the considered alternatives in modeling the data.

6 INAR(1) process with discrete mixture exponential innovations

In this section, the INAR(1) process with innovations following the DME distribution is developed. For this purpose, the INAR(1) model with a binomial thinning operator that employs independent Bernoulli counting series rvs is utilized.

Definition 6.1 The binomial thinning operator is defined as,

$$p \circ X = \sum_{i=1}^{X} B_i, \ p \in (0, 1),$$

where X is a non-negative integer-valued rv and $\{B_i\}$ is a sequence of independent and identically distributed (iid) rvs with Bernoulli (p) distribution and is independent of X.

6.1 INAR(1)DME process

The INAR(1)DME process is given by,

$$X_t = p \circ X_{t-1} + \epsilon_t, \ t \geq 2,$$

Table 3 MLEs with SEs and 95% CI, information criteria and goodness-of-fit measures for the various distributions for corn-borer data

| Distribution		Estimate	SE	95 % CI		logL	AIC	BIC	χ^2	df	p-value
				Lower bound	Upper bound						
DME	α	− 0.3445	0.2925	− 0.9179	0.2288	− 200.3219	404.6439	410.2189	1.1878	3	0.7559
	λ	0.5479	0.0476	0.4545	0.6412						
DB	α	2.3575	0.3656	1.6409	3.0742	− 204.2933	412.5865	418.1615	4.6477	3	0.1995
	θ	0.519	0.0508	0.4194	0.6187						
DG	α	3.11	0.3674	2.39	3.8301	− 213.1911	430.3822	435.9572	10.801	3	0.0129
	p	0.4065	0.0294	0.3489	0.464						
DLL	λ	1.4007	0.1212	1.1631	1.6383	− 202.6303	409.2606	414.8356	2.2441	3	0.5233
	θ	1.9429	0.1879	1.5746	2.3113						
DBL	p	0.6566	0.0186	0.6202	0.693	− 204.6753	411.3505	414.138	6.9961	3	0.072
DP	λ	1.4833	0.1112	1.2654	1.7012	− 219.1879	440.3759	443.1634	21.761	3	0.0001
DPR	α	0.3292	0.0338	0.2629	0.3954	− 220.6182	443.2363	446.0238	35.501	4	0
DR	θ	0.8673	0.0115	0.8448	0.8899	− 235.2266	472.4531	475.2406	60.054	3	0
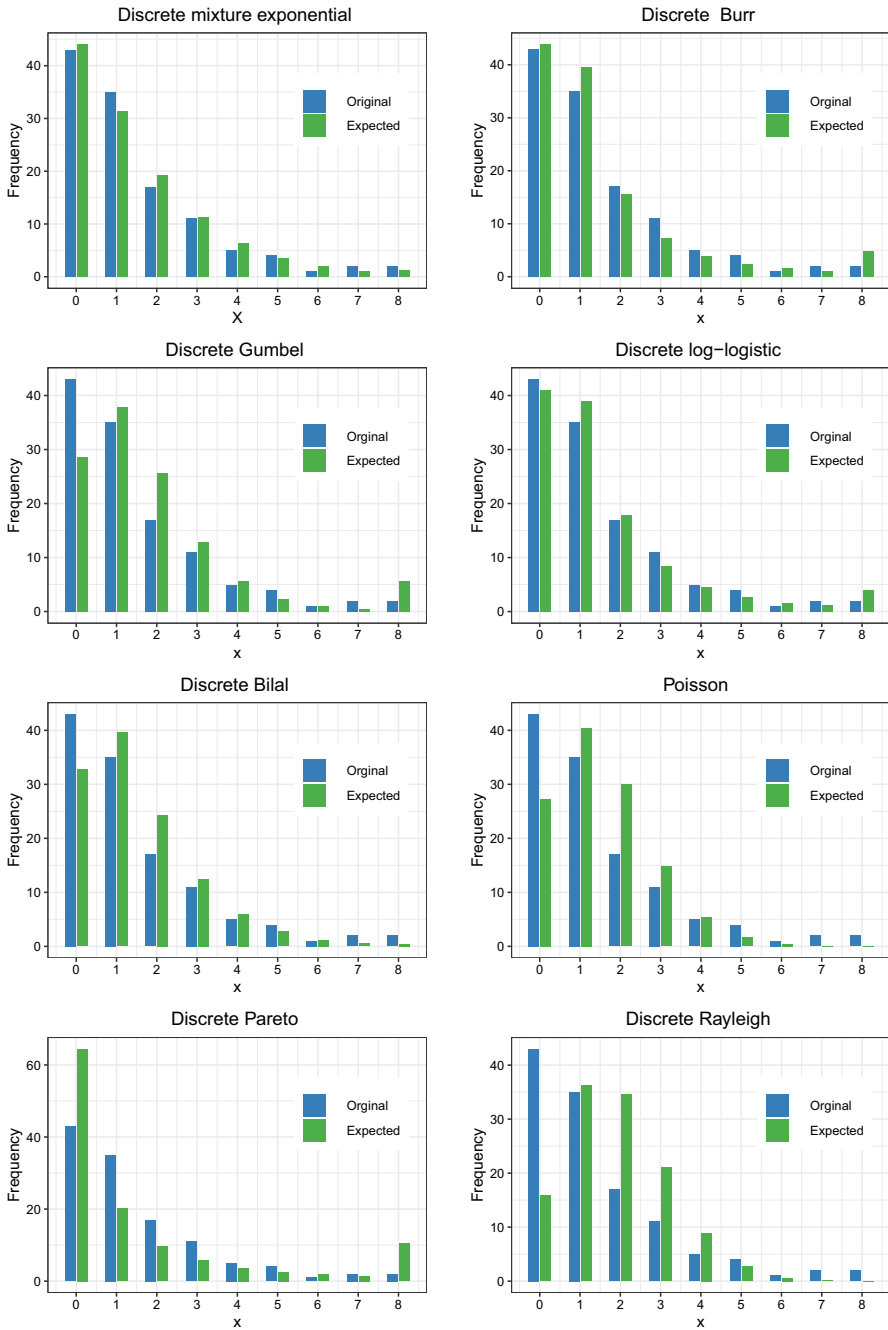
Fig. 5 Observed and expected frequencies of the corn-borer data under various distributions

where "∘" is the binomial thinning operator, $\{\epsilon_t\}$ is a sequence of iid rvs from DME(α, λ) and ϵ_t is independent of Bernoulli counting process $\{B_i\}$ and X_m for all $m \leq t$.

The one-step transition probability of the INAR(1) process is given by,

$$P(X_t = k \mid X_{t-1} = l) = \sum_{i=0}^{\min(k,l)} \binom{l}{i} p^i (1-p)^{l-i} P(\epsilon_t = k - i), \quad k, l \geq 0.$$

Then, the one-step transition probability of the INAR(1)DME process is given by,

$$P(X_t = k \mid X_{t-1} = l) = \sum_{i=0}^{\min(k-l)} \binom{l}{i} p^i (1-p)^{l-i} \{\lambda^{k-i}(1-\lambda)(1-\alpha) + \alpha\lambda^{2k-i}(1-\lambda^2)\}.$$
$$(6.1)$$

Also, the stationary marginal density of $\{X_t\}$ is given by,

$$P(X_t = k) = \sum_{l=0}^{\infty} P(X_t = k \mid X_{t-1} = l) P(X_{t-1} = l)$$

$$= \sum_{l=0}^{\infty} \sum_{i=0}^{\min(k-l)} \binom{l}{i} p^i (1-p)^{l-i} \{\lambda^{k-i}(1-\lambda)(1-\alpha) + \alpha\lambda^{2k-i}(1-\lambda^2)\}.$$
$$(6.2)$$

From Weiß (2018), the mean and variance of $\{X_t\}$ can be computed using (3.1) as,

$$E(X_t) = \mu_X = \frac{(1-\alpha+\lambda)\lambda}{(1-\lambda^2)(1-p)},$$
$$(6.3)$$

$$Var(X_t) = \frac{\lambda([(1+p(1-\lambda))(1+\lambda)^2] - \alpha^2\lambda - \alpha(1+p+\lambda^2-p\,\lambda^2))}{(1-p^2)(1-\lambda^2)^2}.$$
$$(6.4)$$

Then, the DI of $\{X_t\}$ is given by,

$$DI(X_t) = \frac{[(1+p(1-\lambda))(1+\lambda)^2] - \alpha^2\lambda - \alpha(1+p+\lambda^2-p\,\lambda^2)}{(1+p)(1-\lambda^2)(1-\alpha+\lambda)}.$$
$$(6.5)$$

Table 4 provides the DI of $\{X_t\}$ across different parameter configurations, indicating the model's ability to accommodate over-dispersed data. The one-step-ahead conditional mean and variance of the INAR(1)DME process are given by,

$$E(X_t|X_{t-1}) = p\,X_{t-1} + \frac{(1-\alpha+\lambda)\lambda}{(1-\lambda^2)},$$
$$(6.6)$$

$$Var(X_t|X_{t-1}) = p\,(1-p)\,X_{t-1} + \frac{\lambda((1+\lambda)^2 - \alpha^2\lambda - \alpha(1+\lambda^2))}{(1-\lambda^2)^2}.$$
$$(6.7)$$

Table 4 DI of $\{X_t\}$ for various parameter values

$p = 0.4$

λ	α						
	-0.1	-0.5	-0.9	0.9	0.7	0.3	0.1
0.1	1.0734	1.0478	1.0209	1.0794	1.1046	1.0956	1.0851
0.2	1.1683	1.1217	1.0702	1.1339	1.1994	1.2034	1.1880
0.3	1.2927	1.2276	1.1520	1.2002	1.3061	1.3344	1.3179
0.4	1.4603	1.3777	1.2765	1.2925	1.4422	1.5040	1.4893
0.5	1.6964	1.5952	1.4643	1.4286	1.6310	1.7381	1.7279
0.6	2.0517	1.9279	1.7580	1.6409	1.9152	2.0869	2.0848
0.7	2.6449	2.4884	2.2594	2.0049	2.3922	2.6667	2.6789
0.8	3.8321	3.6156	3.2751	2.7460	3.3521	3.8254	3.8665
0.9	7.3947	7.0056	6.3410	4.9925	6.2444	7.3017	7.4286

$p = 0.7$

λ	α						
	-0.1	-0.5	-0.9	0.9	0.7	0.3	0.1
0.1	1.0604	1.0394	1.0172	1.0654	1.0862	1.0787	1.0701
0.2	1.1386	1.1002	1.0578	1.1103	1.1642	1.1675	1.1549
0.3	1.2410	1.1875	1.1252	1.1648	1.2521	1.2754	1.2618
0.4	1.3791	1.3111	1.2277	1.2409	1.3641	1.4151	1.4029
0.5	1.5735	1.4902	1.3824	1.3529	1.5196	1.6078	1.5994
0.6	1.8661	1.7642	1.6243	1.5278	1.7537	1.8951	1.8934
0.7	2.3546	2.2258	2.0372	1.8276	2.1465	2.3725	2.3826
0.8	3.3323	3.1540	2.8736	2.4379	2.9370	3.3268	3.3606
0.9	6.2663	5.9458	5.3985	4.2879	5.3189	6.1896	6.2941

6.2 Estimation

This section discusses the conditional maximum likelihood (CML) and conditional least squares (CLS) parameter estimation for the INAR(1)DME process.

6.2.1 Conditional maximum likelihood

The knowledge of the transition probabilities is sufficient for the creation of the likelihood function in the CML technique. For a given sample $x_1, x_2, ..., x_n$ from the INAR(1)DME process, the conditional log-likelihood function is given by,

$$l(p, \alpha, \lambda) = \sum_{t=2}^{n} \log[P(X_t = x_t \mid X_{t-1} = x_{t-1})], \qquad (6.8)$$

where x_1 is fixed, and $P(X_t = x_t \mid X_{t-1} = x_{t-1})$ is given by (6.1). The CML estimates (CMLEs) of the parameters p, α and λ are obtained by maximizing (6.8) using the `optim` function in R software.

6.2.2 Conditional least squares estimation

The CLS estimates (CLSEs) of parameters p, α and λ are obtained by minimizing the following equation,

$$L(p, \alpha, \lambda) = \sum_{t=2}^{n} (x_t - E(X_t|X_{t-1} = x_{t-1}))^2.$$

To this end, one can use the `optim` function in `R` software.

6.3 Simulation

A simulation study was performed to assess the performance of the CML and CLS estimation methods under the INAR(1)DME process. The simulation is carried out by taking $N = 1000$ replications for samples of sizes $n = 50, 100, 150, 200$, and 250 with different parameter values. The Bias and RMSE are computed accordingly.

Table 5 shows that as n increases, Bias and RMSE decrease for both methods. The CMLEs exhibit lower Bias and RMSE compared to the CLSEs. Hence, the CML estimation method performs very well and is suitable for both small and large sample sizes.

6.4 Empirical study

Here, an example is presented to demonstrate the application of the INAR(1)DME process in fitting a real-world data set.

6.4.1 Methodology

Utilizing model adequacy criteria, the introduced INAR(1)DME process is compared with some existing models. To that end, the existing INAR(1) process with some well-known discrete innovations are used. The following are considered:

- INAR(1) process with Poisson marginals, (Al-Osh and Alzaid 1987) (INARP(1))
- INAR(1) process with negative binomial marginals, (McKenzie 1986) (INARNB(1))
- quasi-binomial INAR(1) process with generalized Poisson marginals, (Alzaid and Al-Osh 1993) (QINARGP(1))
- random coefficient INAR(1) process with negative binomial marginals, (Weiß 2008) (RCINARNB(1))
- iterated INAR(1) process with negative binomial marginals, (Al-Osh and Aly 1992) (IINARNB(1))

Table 5 Simulation results of INAR(1)DME process

CML

n	p			α			λ		
	Estimate	Bias	RMSE	Estimate	Bias	RMSE	Estimate	Bias	RMSE
$p = 0.3,\ \alpha = 0.8,\ \lambda = 0.6$									
50	0.2871	0.0846	0.1052	0.7722	0.2279	0.2653	0.5865	0.0663	0.0828
100	0.2904	0.0588	0.0747	0.7692	0.2010	0.2414	0.5910	0.0554	0.0680
150	0.2942	0.0492	0.0611	0.7772	0.1899	0.2259	0.5935	0.0517	0.0632
200	0.2967	0.0410	0.0510	0.7781	0.1822	0.2193	0.5942	0.0496	0.0603
250	0.2924	0.0382	0.0477	0.7664	0.1834	0.2214	0.5939	0.0494	0.0599
$p = 0.5,\ \alpha = 0.2,\ \lambda = 0.3$									
50	0.4758	0.0915	0.1172	0.2044	0.2371	0.2690	0.3047	0.0650	0.0813
100	0.4884	0.0637	0.0814	0.2299	0.2385	0.2797	0.3089	0.0572	0.0735
150	0.4918	0.0513	0.0644	0.2329	0.2333	0.2797	0.3114	0.0536	0.0692
200	0.4953	0.0432	0.0544	0.2506	0.2312	0.2805	0.3159	0.0524	0.0683
250	0.4940	0.0393	0.0495	0.2448	0.2232	0.2726	0.3149	0.0498	0.0662
$p = 0.2,\ \alpha = -0.6,\ \lambda = 0.4$									
50	0.1953	0.0974	0.1180	− 0.5697	0.3821	0.4713	0.4088	0.0625	0.0798
100	0.1936	0.0716	0.0890	− 0.5881	0.3054	0.3810	0.4044	0.0438	0.0583
150	0.1958	0.0597	0.0738	− 0.6102	0.2715	0.3307	0.4017	0.0376	0.0486
200	0.1996	0.0516	0.0642	− 0.6115	0.2352	0.2993	0.4013	0.0336	0.0454
250	0.1931	0.0470	0.0586	− 0.6213	0.2088	0.2525	0.4005	0.0284	0.0357
$p = 0.3,\ \alpha = -0.4,\ \lambda = 0.7$									
50	0.2832	0.0751	0.0937	− 0.4408	0.4310	0.5110	0.6982	0.0421	0.0543
100	0.2903	0.0539	0.0680	− 0.4046	0.3253	0.4119	0.7022	0.0320	0.0416
150	0.2894	0.0456	0.0569	− 0.4420	0.2746	0.3495	0.6987	0.0265	0.0343
200	0.2948	0.0395	0.0501	− 0.4028	0.2448	0.3157	0.7006	0.0230	0.0309
250	0.2949	0.0358	0.0460	− 0.4116	0.2150	0.2809	0.7004	0.0203	0.0272

CLS

n	p			α			λ		
	Estimate	Bias	RMSE	Estimate	Bias	RMSE	Estimate	Bias	RMSE
$p = 0.3,\ \alpha = 0.8,\ \lambda = 0.6$									
50	0.2634	0.1172	0.1441	0.8146	0.0293	0.0441	0.5345	0.0829	0.1056
100	0.2775	0.0853	0.1050	0.8197	0.0228	0.0293	0.5361	0.0709	0.0884
150	0.2888	0.0701	0.0868	0.8211	0.0225	0.0269	0.5322	0.0717	0.0848
200	0.2902	0.0603	0.0753	0.8213	0.0219	0.0260	0.5330	0.0692	0.0810
250	0.2911	0.0557	0.0696	0.8208	0.0212	0.0248	0.5341	0.0673	0.0779
$p = 0.5,\ \alpha = 0.2,\ \lambda = 0.3$									
50	0.4367	0.1233	0.1559	0.3668	0.1681	0.2312	0.2416	0.0879	0.1074
100	0.4643	0.0888	0.1107	0.3308	0.1309	0.1637	0.2187	0.0899	0.1059
150	0.4779	0.0697	0.0885	0.3188	0.1189	0.1349	0.2094	0.0932	0.1056
200	0.4872	0.0584	0.0736	0.3115	0.1115	0.1185	0.2040	0.0970	0.1063

Table 5 (continued)

CLS

n	p			α			λ		
	Estimate	Bias	RMSE	Estimate	Bias	RMSE	Estimate	Bias	RMSE
250	0.4858	0.0560	0.0703	0.3121	0.1121	0.1175	0.2048	0.0961	0.1051
$p = 0.2,\ \alpha = -0.6,\ \lambda = 0.4$									
50	0.1769	0.1096	0.1312	− 0.4702	0.1469	0.1861	0.3708	0.0613	0.0769
100	0.1851	0.0861	0.1048	− 0.4690	0.1376	0.1646	0.3663	0.0519	0.0645
150	0.1901	0.0679	0.0849	− 0.4698	0.1348	0.1541	0.3654	0.0458	0.0565
200	0.1949	0.0591	0.0740	− 0.4717	0.1299	0.1469	0.3639	0.0436	0.0534
250	0.1905	0.0555	0.0696	− 0.4734	0.1277	0.1423	0.3657	0.0407	0.0499
$p = 0.3,\ \alpha = -0.4,\ \lambda = 0.7$									
50	0.2579	0.1103	0.1367	− 0.2817	0.1197	0.1484	0.6446	0.0757	0.0981
100	0.2824	0.0789	0.0981	− 0.2804	0.1199	0.1360	0.6367	0.0702	0.0872
150	0.2871	0.0616	0.0762	− 0.2819	0.1182	0.1285	0.6360	0.0666	0.0794
200	0.2924	0.0591	0.0739	− 0.2785	0.1215	0.1309	0.6329	0.0689	0.0815
250	0.2932	0.0509	0.0640	− 0.2809	0.1191	0.1263	0.6338	0.0672	0.0773

- negative binomial thinning-based INAR(1) process with geometric marginals, (Ristić et al. 2009) (NBINARG(1))
- INAR(1) process with geometric marginals, (Alzaid and Al-Osh 1988) (INARG(1))
- dependent counting INAR(1) process with geometric marginals, (Ristić et al. 2013) (DCINARG(1))
- INAR(1) process with zero-inflated Poisson innovations, (Jazi et al. 2012b) (INAR(1)ZP)
- INAR(1) process with geometric innovations, (Jazi et al. 2012a) (INAR(1)G)
- INAR(1) process with Katz family innovations, (Kim and Lee 2017) (INAR(1) KF)

The CML method is employed for parameter estimation. Subsequently, logL, AIC, BIC, and RMSE* for all the models described above are computed.. The RMSE* measures the differences between true values and one-step conditional expectation and is given by,

$$\text{RMSE}^* = \sqrt{\frac{1}{N} \sum_{n=1}^{N} \left(x_n - \hat{x}_n \right)^2},$$

where $\hat{x}_n$, $n = 1, 2, \ldots, N$, is the predicted value, which is the realization of $\hat{X}_t$ and are given by,

$$\hat{X}_1 = E(X_t)_{\hat{\theta}_{\mathrm{CML}}},$$

$$\hat{X}_t = E(X_t \mid X_{t-1})_{\hat{\theta}_{\mathrm{CML}}}, \ t = 2, \ldots, n,$$

where $\hat{\theta}_{\mathrm{CML}}$ is the CMLE of the parameter vector (p, α, λ). A model exhibiting a large logL along with small AIC and BIC values offers the optimal fit to the data. Additionally, it holds the potential for good forecasts if its RMSE* is the minimum among the models under consideration.

Further, the standardized Pearson residuals are used to check whether the INAR(1)DME process is a good fit for the data set. They are calculated using the following formula:

$$r_t = \frac{x_t - E(x_t \mid X_{t-1} = x_{t-1})}{V(x_t \mid X_{t-1} = x_{t-1})^{1/2}},$$

where $E(X_t|X_{t-1})$ and $Var(X_t|X_{t-1})$ are given in (6.6) and (6.7), respectively. If the INAR(1) process is well-fitted, then the Pearson residuals are uncorrelated and have zero mean and unit variance (Harvey and Fernandes 1989). The residuals autocorrelation function (ACF) is plotted to see if they are uncorrelated.

6.4.2 Burglary data set

The burglary data from the Forecasting Principles site

(http://www.forecastingprinciples.com), which was used to fit the INAR(1)KF process introduced by Kim and Lee (2017) is considered here for demonstrating the capability of the introduced model. The data set contains 144 observations from January 1990 to December 2001, and it provides monthly counts of burglaries in the 65th police car beat in Pittsburgh. The mean and variance of this data set are 5.9583 and 17.8304, respectively.

Figure 6 depicts the burglary data set's time series plot. The ACF and partial ACF (PACF) plots are displayed in Fig. 7. Here, only the first lag is significant in the PACF plot, and the ACF plot displays an exponential decay, facilitating to model the data as an INAR(1) process.

Table 6 lists the CMLEs, logL, AIC, BIC and RMSE*, for different processes. The maximum value of logL and minimum values of AIC and BIC for the INAR(1)DME process prove that it provides a better fit than the contending models. Also, it can provide a good forecast since the RMSE* value is the lowest among the considered models. Hence, it is convincing that the INAR(1)DME process effectively explains the data set's characteristics.

To check whether the fitted INAR(1)DME process is statistically accurate, residual analysis is done with the Pearson residuals. The ACF of the Pearson residuals is displayed in Fig. 8, showing no autocorrelation for the Pearson residuals. To ensure this, the Ljung-Box test for the presence of autocorrelation is done with degrees of freedom 10 and has the p-value $= 0.0771 > 0.05$. It indicates that the residuals are uncorrelated. Also, the mean and variance of Pearson residuals
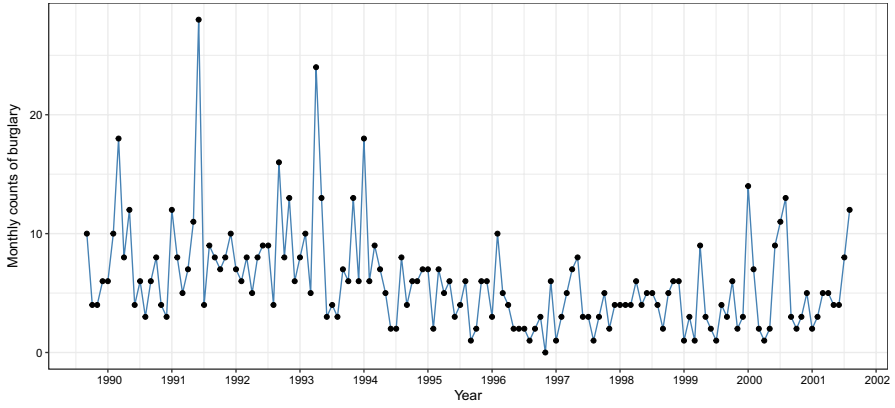
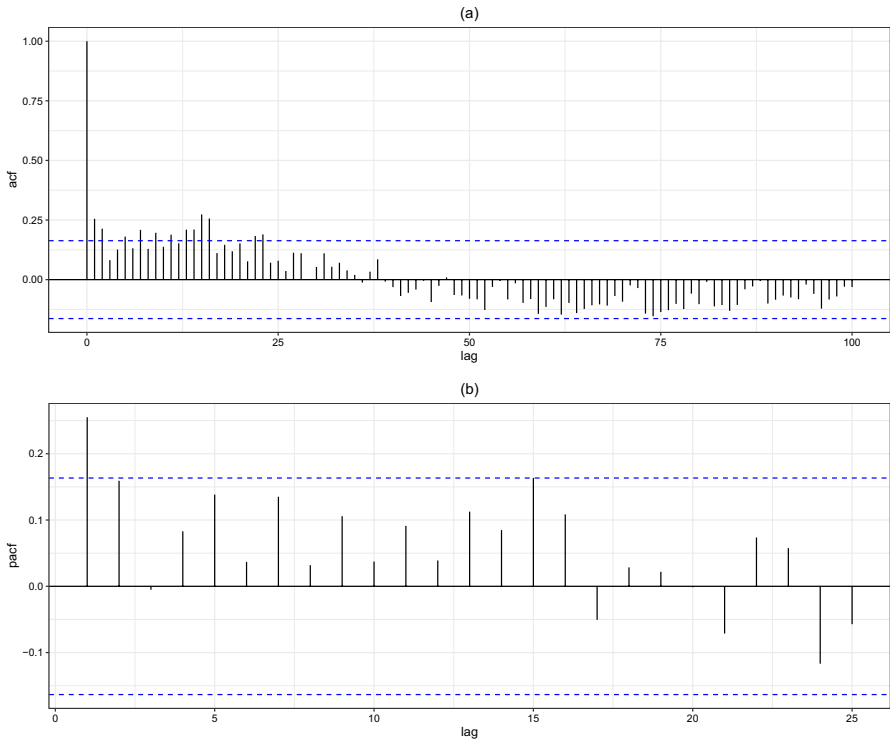**Fig. 6** The time series plot of the burglary data set

Fig. 7 The ACF (**a**) and PACF (**b**) plot for the burglary data set

Table 6 The CMLEs, logL, AIC, BIC and RMSE* of the considered processes for the burglary data set

Model	Parameter	CMLE	logL	AIC	BIC	RMSE*
INAR(1)DME	p	0.2551	− 369.7776	745.5551	754.4646	4.0669
	α	− 0.9999				
	λ	0.7368				
INARG(1)	π	0.204	− 379.245	762.49	768.43	4.092
	α	0.3629				
NGINAR(1)	μ	5.3233	− 392.275	788.55	794.49	4.343
	α	0.6165				
GINAR(1)	p	0.1787	− 403.185	810.37	816.31	4.178
	ρ	0.3605				
PINAR(1)	λ	4.9021	− 421.135	846.27	852.21	4.081
	α	0.1794				
NBINAR(1)	n	4.0768	− 375.76	757.52	766.43	4.067
	p	0.4058				
	ρ	0.256				
GPQINAR(1)	λ	3.7243	− 374.56	755.12	764.03	4.085
	θ	0.3944				
	ρ	0.3448				
NBRCINAR(1)	n	3.7878	− 375.755	757.51	766.41	4.081
	p	0.3825				
	ρ	0.3339				
NBIINAR(1)	n	3.9045	− 375.94	757.88	766.72	4.071
	α	0.9346				
	ρ	0.3024				
DCGINAR(1)	μ	4.9605	− 399.295	804.59	813.5	4.177
	α	0.4447				
	θ	0.436				
ZINAR(1)	λ	4.961	− 411.905	829.81	838.72	4.091
	ρ	0.2276				
	α	0.3628				
INARKF(1)	θ_1	1.4834	− 374.45	754.9	763.81	4.067
	θ_2	0.6634				
	α	0.2585				

are 0.00183 and 1.1235, close to the preferred values 0 and 1, respectively, validating a good fit. Hence, the INAR(1)DME process fits the burglary data set.

The INAR(1)DME model for the burglary data set is given by,

$$X_t = 0.2551 \circ X_{t-1} + \epsilon_t, \ t \geq 2,$$

where $\epsilon_t \sim DME(-0.9999, 0.7368)$.
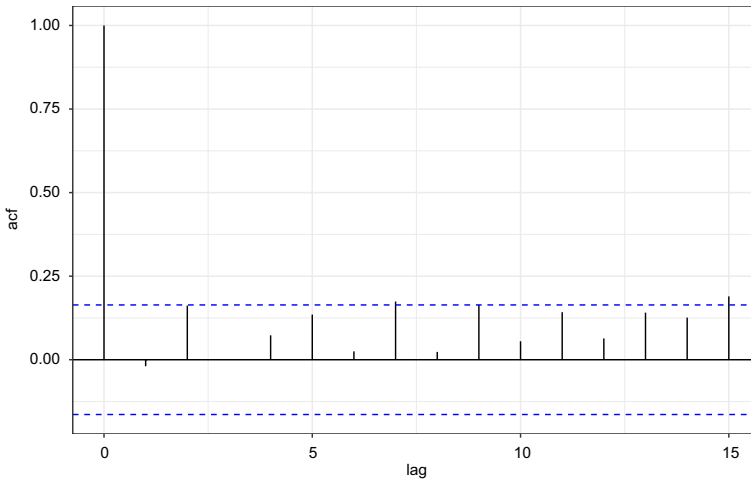
The predicted values can be obtained by

Fig. 8 The ACF plot of the Pearson residuals

$$\hat{x}_1 = 5.9223.$$
$$\hat{x}_t = 0.2551\,\hat{x}_{t-1} + 4.4118,\ t = 2, 3, \ldots, 144.$$

7 Control charts for monitoring mean of the INAR(1)DME process

This section explores an efficient control chart for monitoring the mean of the INAR(1)DME process. In INAR(1) processes, upward shifts in the process mean indicate a collective rise in associated factors for entities, such as unemployment rate, defect percentage, and disease spread. Identification and timely reporting of such shifts are typically vital. Therefore, focusing on practical applications, this session investigates the mean upward shift within the INAR(1)DME process.

Here, the upper-sided control chart is constructed by exclusively focusing on detecting upward shifts in μ_X, as they are directly linked to process deterioration. The primary purpose is to detect quickly and accurately a change in the μ_X. It is more intuitive to directly monitor the process $\{X_t\}$ while accounting for the impact of autocorrelation. A process is considered in control when it adheres to a specified model. Conversely, a process is deemed out of control when the parameters within the model change rather than the model itself changing. When the process is in control, the parameter values of the INAR(1)DME process will be denoted as p_0, α_0, and λ_0. An increasing shift in μ_X may occur if one of the parameters p, α and λ have changed appropriately.

It is clearly seen in Table 7 that μ_X is affected by variations in the parameters within the INAR(1)DME process. Also, with a rise in p and λ, there is an increase in the value of μ_X, and with a rise in α in the intervals $[-0.9, -0.1]$ and $[0.1, 0.9]$,

Table 7 Mean of $\{X_t\}$ of INAR(1)DME process

λ	α									
	− 0.1	− 0.3	− 0.5	− 0.7	− 0.9	0.9	0.7	0.5	0.3	0.1
$p = 0.4$										
0.1	0.202	0.236	0.269	0.303	0.337	0.034	0.067	0.101	0.135	0.168
0.2	0.451	0.521	0.59	0.66	0.729	0.104	0.174	0.243	0.312	0.382
0.3	0.769	0.879	0.989	1.099	1.209	0.22	0.33	0.44	0.549	0.659
0.4	1.19	1.349	1.508	1.667	1.825	0.397	0.556	0.714	0.873	1.032
0.5	1.778	2	2.222	2.444	2.667	0.667	0.889	1.111	1.333	1.556
0.6	2.656	2.969	3.281	3.594	3.906	1.094	1.406	1.719	2.031	2.344
0.7	4.118	4.575	5.033	5.49	5.948	1.83	2.288	2.745	3.203	3.66
0.8	7.037	7.778	8.519	9.259	10	3.333	4.074	4.815	5.556	6.296
0.9	15.789	17.368	18.947	20.526	22.105	7.895	9.474	11.053	12.632	14.211
$p = 0.7$										
0.1	0.404	0.471	0.539	0.606	0.673	0.067	0.135	0.202	0.269	0.337
0.2	0.903	1.042	1.181	1.319	1.458	0.208	0.347	0.486	0.625	0.764
0.3	1.538	1.758	1.978	2.198	2.418	0.44	0.659	0.879	1.099	1.319
0.4	2.381	2.698	3.016	3.333	3.651	0.794	1.111	1.429	1.746	2.063
0.5	3.556	4	4.444	4.889	5.333	1.333	1.778	2.222	2.667	3.111
0.6	5.312	5.937	6.562	7.187	7.812	2.187	2.812	3.437	4.062	4.687
0.7	8.235	9.15	10.065	10.98	11.895	3.66	4.575	5.49	6.405	7.32
0.8	14.074	15.556	17.037	18.519	20	6.667	8.148	9.63	11.111	12.593

there is a decrease in the values of μ_X. So, to effectively monitor INAR(1) processes, CUSUM and EWMA control charts are employed and their efficiency is assessed.

7.1 The CUSUM chart

Initially proposed by Page (1961), the CUSUM chart operates on the fundamental principle of the sequential probability ratio test. Its primary objective is to gather and accumulate information from sample data, thus magnifying the impact of minor process deviations. Numerous studies have extensively demonstrated the effectiveness of the CUSUM chart in monitoring time series comprising integer values, including Poisson INAR(1) by Weiß and Testik (2009) and Weiß and Testik (2011), geometrically inflated Poisson INAR(1) by Li et al. (2022), and zero-inflated Poisson INAR(1) by Rakitzis et al. (2017).

Here, the CUSUM control chart is devised due to their sensitivity in detecting small shifts. Furthermore, CUSUM charts also have known optimality properties when detecting a sustained shift from a known in control distribution to a specified out of control distribution (Weiß and Testik 2009).

From Weiß and Testik (2009), let $C_0 = c_0$, $c_0 \in N_0$. A CUSUM statistic with reference value k is obtained as,

$$C_t = max(0, X_t - k + C_{t-1}), \ t = 1, 2, \ldots$$

Here $c_o \geq 0$ is the starting value. For $\mu_X < k < h$, the monitoring statistics $\{C_t\}$ are plotted on a CUSUM chart with control region $[0, h]$, where h is the upper control limit. The INAR(1)DME process is considered as being in control unless $C_t > h$. The reference value k prevents the chart from drifting towards control limits during in control processes and offers the ability to fine-tune chart sensitivity to specific shifts in the process mean.

7.2 The EWMA chart

Initially proposed by Roberts (2000), the EWMA chart operates on the fundamental principle of giving the highest weight to the nearest samples in the time series while previous samples contribute minimally. The EWMA chart is useful for detecting persistent shifts for INAR processes (Weiß 2009).

From Weiß (2011), let $Q_0 = q_0$, $q_0 \in \{0, 1, ..., u - 1\}$ and $\theta \in (0, 1]$. An EWMA statistic of the INAR(1) process is given by,

$$Q_t = round(\theta \, X_t + (1 - \theta) \, Q_{t-1}), \ t \in N_0,$$

where $round(x) = z$ if and only if the integer $z \in (x - 1/2, x + 1/2]$. Let $u \in N$ with $u > 1$. The statistics Q_t are plotted on an EWMA chart with control region $[1, u]$, where u is the upper control limit. The process is considered in control unless an out of control signal $Q_t \geq u$ is triggered.

7.3 Performance of the INAR(1)DME control charts

The ARL is a commonly used measure to evaluate the effectiveness of a control chart in statistical process control. It represents the expected number of data points plotted on the control chart before it signals an out of control condition. Two specific types of ARL are considered: ARL_0, also known as in control ARL, measures the number of data points plotted from the beginning of monitoring until a false alarm is triggered. On the other hand, ARL_1, referred to as out of control ARL, quantifies the number of data points plotted from the start of a process shift until the chart detects that shift. To have an effective control chart, a high ARL_0 combined with a small ARL_1 is essential.

7.3.1 ARL of CUSUM chart

For a given $C_0 = c_0$, the values of (k, h) are chosen to ensure that the ARL_0 closely matches a specified value. As $\{X_t, C_t\}$ of the INAR(1)DME process forms a bivariate Markov chain, the Markov chain approach introduced in Weiß and Testik (2009) is used here for computing ARL. To offer a comprehensive overview, the computational approach is briefly outlined as follows.

Let us consider the case where h, k, $c_0 \in N_0$. Whenever $X_t > k + h$, it leads to an out of control signal since C_t exceeds h if and only if $X_t - k + C_{t-1} \geq h$. Hence, the attainable in control range of (X_t, C_t) needs to be restricted. From Weiß and Testik (2009), under the CUSUM chart, the set of attainable in control values for the bivariate Markov process $\{X_t, C_t\}$ is given by,

$$\mathcal{CR} = \{(x, i) \mid 0 \leq i \leq h - 1, \; max(0, i + k - h + 1) \leq x \leq i + k\},$$

which is of size

$$|\mathcal{CR}| = \frac{1}{2}(h - k)(h + k + 1) + hk. \tag{7.1}$$

The above arguments can also be extended if h, k and c_0 are permitted to assume values from the set $\{r/s \mid r \in \mathbb{N}_0\}$, where the common denominator $s \in \mathbb{N}, s > 1$.

From Li et al. (2022), the transition probability matrix of (X_t, C_t) is expressed as,

$$Q^\top \triangleq (p(n, j \mid m, i))_{(n,j),(m,i) \, \in \, \mathcal{CR}},$$

where

$$
\begin{aligned}
p(n, j \mid m, i) &\triangleq P(X_t = n, C_t = j \mid X_{t-1} = m, C_{t-1} = i) \\
&= P(C_t = j \mid X_t = n, X_{t-1} = m, C_{t-1} = i) \, P(X_t = n \mid X_{t-1} = m, C_{t-1} = i) \\
&= \delta_{j, max(0, n-k+i)} \, P(X_t = n \mid X_{t-1} = m).
\end{aligned}
$$

The initial probabilities are,

$$
\begin{aligned}
p(m, i \mid c_0) &\triangleq P(X_1 = m, C_1 = i \mid C_0 = c_0) \\
&= P(C_1 = i \mid X_1 = m, C_0 = c_0) \, P(X_1 = m \mid C_0 = c_0) \\
&= \delta_{i, max(0, m-k+c_0)} \, P(X_1 = m),
\end{aligned}
$$

where $\delta_{x,y}$ denotes the Kronecker delta, $P(X_t = i \mid X_{t-1} = j)$ and $P(X_1 = m)$ are given by (6.1) and (6.2) respectively.

Also, the conditional probability that the run length of $\{X_t, Q_t\}$ equals r is given by,

$$p_{m,i}(r) \triangleq P((X_{r+1}, C_{r+1}) \notin \mathcal{CR}, (X_r, C_r), \ldots, (X_2, C_2) \in \mathcal{CR} \mid (X_1, C_1) = (m, i)),$$

where $(m, i) \in \mathcal{CR}$.

Let the vector $\mu_{(l)}$ denote the lth factorial moments, given by,

$$\mu_{(l)_{m,i}} \triangleq \sum_{r=1}^{\infty} r \cdots (r - l + 1) \, p_{m,i}(r), \; l \geq 1,$$

where,

$$p_{m,i}(r) = \sum_{(n,j)\in\mathcal{CR}} p_{n,j}(r-1)\, p(n,j \mid m,i).$$

Then,

$$\mu_{(1)_{m,i}} = 1 + \sum_{(n,j)\in\mathcal{CR}} p(n,j \mid m,i)\, \mu_{(1)_{n,j}}.$$

That is, $\mu_{(1)}$ is the solution of the linear equation $(I - Q)\mu_{(1)} = 1$. The dimension of Q and μ is determined by (7.1). Hence, the ARL depending on the initial choice $C_0 = c_0$, is defined as,

$$ARL(c_0) = 1 + \sum_{(m,i)\in\mathcal{CR}} \mu_{(1)_{m,i}}\, p(m,i \mid c_0).$$

7.3.2 ARL of EWMA chart

For a given $Q_0 = q_0$, the values of (θ, u) are chosen to ensure that the ARL_0 closely matches a specified value. Subsequently, the ARL values are calculated using the model parameters and EWMA chart designs. As $\{X_t, Q_t\}$ of the INAR(1)DME process forms a bivariate Markov chain, the Markov chain approach introduced in Weiß (2011) is used here for computing ARL. To offer a comprehensive overview, the computational approach is briefly outlined as follows.

Let $[x]$ denote the smallest integer value greater than or equal to x. From Weiß (2011), under the EWMA chart, the set of attainable in control values for the bivariate Markov process $\{X_t, Q_t\}$ is given by,

$$\mathcal{I}(u,\theta) = \left\{(n,q) \in \left\{0,\dots,\left[\frac{1}{\theta}\left(u - \frac{1}{2}\right) - 1\right]\right\} \times \{0,\dots,u-1\} \mid \right.$$
$$\left. \left[\frac{1}{\theta}\left(q - \frac{1}{2} - (1-\theta)(u-1)\right)\right] \le n \le \left[\frac{1}{\theta}\left(q + \frac{1}{2}\right) - 1\right]\right\}. \tag{7.2}$$

The transition probabilities of $\{X_t, Q_t\}$ is given by,

$$Q^{\mathsf{T}} \triangleq (p(n,j|m,i))_{(n,j),(m,i)\,\in\,\mathcal{I}(u,\theta)} \tag{7.3}$$

where

$$p(n,j \mid m,i) \triangleq P\big(X_t = n, Q_t = j \mid X_{t-1} = m, Q_{t-1} = i\big)$$
$$= \mathbf{I}_{[j-1/2;j+1/2)}\,(\theta\, n + (1-\theta)\, i)\, P\big(X_t = n \mid X_{t-1} = m\big).$$

The initial probabilities are,

$$p\big(m,i \mid q_0\big) \triangleq P\big(X_1 = m, Q_1 = i \mid Q_0 = q_0\big)$$
$$= \mathbf{I}_{[j-1/2;j+1/2)}\,(\theta\, n + (1-\theta)\, q_0)\, P\big(X_1 = m\big),$$

where $\mathbf{I}_A$ denote the indicator function.

Also, the conditional probability that the run length of $\{X_t, Q_t\}$ equals r is given by,

$$p_{m,i}(r) \triangleq P\big((X_{r+1}, Q_{r+1}) \notin \mathcal{I}(u, \theta), (X_r, Q_r), \ldots, (X_2, Q_2) \in \mathcal{I}(u, \theta) \mid (X_1, Q_1) = (m, i)\big),$$

where $(m, i) \in \mathcal{I}(u, \theta)$.

Then, the lth factorial moment is given by,

$$\mu_{(l)_{m,i}} \triangleq \sum_{r=1}^{\infty} r \cdots (r - l + 1)\, p_{m,i}(r), \ l \geq 1, \tag{7.4}$$

where

$$p_{m,i}(r) = \sum_{(n,j)\,\in \mathcal{I}(u,\theta)} p_{n,j}(r - 1)\, p(n, j \mid m, i).$$

Then,

$$\mu_{(1)_{m,i}} = 1 + \sum_{(n,j)\in\mathcal{I}(u,\theta)} p(n, j \mid m, i)\, \mu_{(1)_{n,j}}.$$

That is, $\mu_{(1)}$ is the solution of the linear equation $(I - Q)\mu_{(1)} = 1$.

Hence, the *ARL* depending on the initial choice $Q_0 = q_0$, is defined as,

$$ARL(q_0) = 1 + \sum_{(m,i)\in\mathcal{I}(u,\theta)} \mu_{(1)_{m,i}}\, p(m, i \mid q_0).$$

7.4 Numerical simulation

Here, the performance of both CUSUM and EWMA in detecting changes in the process mean is assessed by employing a simulation study. The primary objective is to recognize the effect of parameters leading to changes in μ_X. Table 8 presents a comprehensive depiction of the variability observed in μ_X across various values of the parameter α with respect to $\alpha_0 = -0.1$ and 0.9.

The deviations are calculated according to,

$$dev_{\mu}^{\%} = 100\% \times \frac{(\mu_X - \mu_0)}{\mu_0},$$

where μ_0 is the mean associated with the parameters p_0, α_0 and λ_0.

Table 8 shows that if the value of α is decreased by 0.2, there is more than a 10% increase in μ_X under the considered α_0.

The control chart designs are determined in such a way that the desired in control ARL value, ARL_0, is 300. Due to the complexity of (6.2), the marginal probabilities are empirically obtained through a simulated process of desirable size at given (p, α, λ). Besides ARL as a performance measure for the control charts, the usual

Table 8 Deviations of mean of INAR(1)DME process with in control values of α

$P_0 = 0.4$ and $\alpha_0 = -0.1$

λ_0	-0.1	-0.3	-0.5	-0.7	-0.9
0.4	1.19	1.349 (13.36%)	1.508 (26.72%)	1.667 (40.08%)	1.825 (53.36%)
0.49	1.709	1.924 (12.58%)	2.139 (25.16%)	2.354 (37.74%)	2.569 (50.32%)
0.6	2.656	2.969 (11.78%)	3.281 (23.53%)	3.594 (35.32%)	3.906 (47.06%)
0.65	3.283	3.658 (11.42%)	4.033 (22.84%)	4.408 (34.27%)	4.784 (45.72%)
0.77	5.895	6.525 (10.69%)	7.156 (21.39%)	7.786 (32.08%)	8.417 (42.78%)
0.9	15.789	17.368 (10.00%)	18.947 (20.00%)	20.526 (30.00%)	22.105 (40.00%)

$P_0 = 0.7$ and $\alpha_0 = 0.9$

λ_0	0.9	0.7	0.5	0.3	0.1
0.4	0.794	1.111 (39.92%)	1.429 (79.97%)	1.746 (119.90%)	2.063 (159.82%)
0.49	1.268	1.698 (33.91%)	2.128 (67.82%)	2.558 (101.74%)	2.988 (135.65%)
0.6	2.187	2.812 (28.58%)	3.437 (57.16%)	4.062 (85.73%)	4.687 (114.31%)
0.65	2.814	3.564 (26.65%)	4.315 (53.34%)	5.065 (79.99%)	5.815 (106.65%)
0.77	5.485	6.746 (22.99%)	8.007 (45.98%)	9.268 (68.97%)	10.529 (91.96%)
0.9	15.789	18.947 (20.00%)	22.105 (40.00%)	25.263 (60.00%)	28.421 (80.01%)

relative deviation (RD) of the ARL from Weiß and Testik ([2011](#)) is also incorporated to assess and evaluate the efficacy and performance of the chart. It is given by,

$$\text{RD} = 100\% \times \frac{(\text{ARL} - \text{ARL}_0)}{\text{ARL}_0}.$$

Under the CUSUM chart, for a given $C_0 = c_0$, the focus revolves around possible integer h and k pairs, such that the desired in control ARL is close to ARL_0. For the EWMA chart, the design parameters are obtained as follows:

- Choose $u \in N$ such that a corresponding one-sided C chart would have an in control ARL below the desired value ARL_0.
- Decrease $\theta \in (0, 1]$ to adjust the in control ARL close to the desired value ARL_0. Subsequently, $l = 0$ in the combined EWMA chart is calculated accordingly as $l = \left\lfloor \frac{1}{2\theta} \right\rfloor$, to keep an upper-sided design minimal.
- Use $q_0 \in \{0, ..., u - 1\}$ for a fine-tuning of the in control ARL.

Subsequently, the ARL values are calculated using the model parameters and chart designs.

In Tables [9](#) and [10](#), the performance of ARL under CUSUM chart is examined with $\alpha_0 = (-0.1, 0.9)$ with various values of α respectively. The results show the high efficacy of the CUSUM chart in detecting upward shifts in μ_X. For example, with a 13.36% and 39.92% increase in μ_X ($\lambda_0 = 0.4$), the ARL decreases by approximately around 37.80% and 64.87%, respectively, signifying a notable decline as μ_X rises. Furthermore, it is important to note that the decline in ARL is significantly greater than the corresponding rise in the magnitude of the shift in μ_X. Hence, it can be concluded that the CUSUM control chart demonstrates effective performance when applied to the INAR(1)DME process. The chart's ability to efficiently detect upward shifts in μ_X makes it a suitable and beneficial tool for monitoring and controlling the INAR(1)DME process.

In Tables [11](#) and [12](#), the performance of ARL under EWMA chart is examined with
$\alpha_0 = (-0.1, 0.9)$ against various values of α, respectively. The results show the high efficacy of the EWMA chart in detecting upward shifts in μ_X. For example, with a 13.36% and 39.92% increase in μ_X ($\lambda_0 = 0.4$), the ARL decreases by approximately 26.05% and 63.11%, respectively, signifying a notable decline as μ_X rises. Furthermore, it is important to note that the decline in ARL is significantly greater than the corresponding rise in the magnitude of the shift in μ_X. Hence, it can be concluded that the EWMA control chart demonstrates effective performance when applied to the INAR(1)DME process. The chart's ability to efficiently detect upward shifts in μ_X makes it a suitable and beneficial tool for monitoring and controlling the INAR(1)DME process.

Table [13](#) provides a comparative analysis of CUSUM and EWMA charts within the context of the INAR(1)DME process, considering specific values of α_0. Bolded entries indicate instances where the RD is maximized between the two charts

Table 9 ARL with deviation (in parenthesis) for the CUSUM charts with $p_0 = 0.4$ and $\alpha_0 = -0.1$

λ_0	k	h	c_0	λ	α				
					-0.1	-0.3	-0.5	-0.7	-0.9
0.4	2	10	0	0.4	308.03	191.61	125.81	86.53	62.01
						(-37.80%)	(-59.16%)	(-71.91%)	(-79.87%)
	2	10	0	0.49	60.99	42.36	31.12	23.92	19.1
						(-80.20%)	(-86.25%)	(-89.90%)	(-92.23%)	(-93.80%)
	2	10	0	0.6	16.83	13.36	11.02	9.35	8.11
						(-94.54%)	(-95.66%)	(-96.42%)	(-96.96%)	(-97.37%)
	3	5	0	0.4	294.83	208.65	153	115.41	89.09
						(-29.23%)	(-48.11%)	(-60.85%)	(-69.78%)
	3	5	0	0.49	67.89	50.25	38.51	30.34	24.46
						(-76.97%)	(-82.96%)	(-86.94%)	(-89.71%)	(-91.70%)
	3	5	0	0.6	17.97	14.26	11.65	9.76	8.33
						(-93.90%)	(-95.16%)	(-96.05%)	(-96.69%)	(-97.17%)
	2	10	4	0.4	300.25	184.7	119.6	80.89	56.85
						(-38.48%)	(-60.17%)	(-73.06%)	(-81.07%)
	2	10	4	0.49	56.71	38.5	27.61	20.71	16.13
						(-81.11%)	(-87.18%)	(-90.80%)	(-93.10%)	(-94.63%)
	2	10	4	0.6	14.53	11.27	9.1	7.58	6.46
						(-95.16%)	(-96.25%)	(-96.97%)	(-97.48%)	(-97.85%)
0.65	5	20	0	0.65	288.72	174.69	111.65	74.87	52.46
						(-39.50%)	(-61.33%)	(-74.07%)	(-81.83%)
	5	20	0	0.77	19.5	15.05	12.13	10.1	8.63
						(-93.25%)	(-94.79%)	(-95.80%)	(-96.50%)	(-97.01%)
	5	20	0	0.9	3.96	3.55	3.22	2.95	2.73
						(-98.63%)	(-98.77%)	(-98.88%)	(-98.98%)	(-99.05%)
	7	11	0	0.65	309.75	215.68	155.5	115.27	87.42
						(-30.37%)	(-49.80%)	(-62.79%)	(-71.78%)
	7	11	0	0.77	22.56	17.46	13.96	11.46	9.61
						(-92.72%)	(-94.36%)	(-95.49%)	(-96.30%)	(-96.90%)
	7	11	0	0.9	3.58	3.17	2.85	2.58	2.37
						(-98.84%)	(-98.98%)	(-99.08%)	(-99.17%)	(-99.23%)
	7	11	4	0.65	307.21	213.37	153.39	113.33	85.62
						(-30.55%)	(-50.07%)	(-63.11%)	(-72.13%)
	7	11	4	0.77	21.61	16.57	13.13	10.66	8.85
						(-92.97%)	(-94.61%)	(-95.73%)	(-96.53%)	(-97.12%)
	7	11	4	0.9	3.25	2.85	2.54	2.29	2.08
						(-98.94%)	(-99.07%)	(-99.17%)	(-99.25%)	(-99.32%)

sharing the same model parameters. It becomes evident that both charts exhibit a more significant reduction in ARL as μ_x increases. When comparing the RD between CUSUM and EWMA charts (e.g., (−38.48%, −34.29%), (−39.50%, −35.83%)),

Table 10 ARL with deviation (in parenthesis) for the CUSUM charts with $p_0 = 0.4$ and $\alpha_0 = 0.9$

λ_0	k	h	c_0	λ	α				
					0.9	0.7	0.5	0.3	0.1
0.4	1	5	0	0.4	320.07	112.44	60.28	38.46	27.12
						(-64.87%)	(-81.17%)	(-87.98%)	(-91.53%)
	1	5	0	0.49	86.79	39.97	24.74	17.5	13.37
					(-72.88%)	(-87.51%)	(-92.27%)	(-94.53%)	(-95.82%)
	1	5	0	0.6	24.1	15.05	10.92	8.57	7.06
					(-92.47%)	(-95.30%)	(-96.59%)	(-97.32%)	(-97.79%)
	1	5	2	0.4	315.34	109.18	57.59	36.1	24.99
					(-65.38%)	(-81.74%)	(-88.55%)	(-92.08%)	
	1	5	2	0.49	83.67	37.72	22.86	15.84	11.88
					(-73.47%)	(-88.04%)	(-92.75%)	(-94.98%)	(-96.23%)
	1	5	2	0.6	22.16	13.58	9.68	7.48	6.08
					(-92.97%)	(-95.69%)	(-96.93%)	(-97.63%)	(-98.07%)
	1	5	4	0.4	297.06	98.92	50.15	30.23	20.17
					(-66.70%)	(-83.12%)	(-89.82%)	(-93.21%)	
	1	5	4	0.49	74.35	32.01	18.62	12.46	9.06
					(-74.97%)	(-89.22%)	(-93.73%)	(-95.81%)	(-96.95%)
	1	5	4	0.6	17.85	10.63	7.41	5.63	4.51
					(-93.99%)	(-96.42%)	(-97.51%)	(-98.10%)	(-98.48%)
0.65	2	16	0	0.65	286.98	87.72	44.66	28.34	20.34
					(-69.43%)	(-84.44%)	(-90.12%)	(-92.91%)	
	2	16	0	0.77	23.6	15.37	11.46	9.18	7.68
					(-91.78%)	(-94.64%)	(-96.01%)	(-96.80%)	(-97.32%)
	2	16	0	0.9	5.03	4.35	3.83	3.42	3.09
					(-98.25%)	(-98.48%)	(-98.67%)	(-98.81%)	(-98.92%)
	3	9	0	0.65	292.12	99.56	53.06	33.69	23.63
					(-65.92%)	(-81.84%)	(-88.47%)	(-91.91%)	
	3	9	0	0.77	27.81	16.35	11.49	8.82	7.15
					(-90.48%)	(-94.40%)	(-96.07%)	(-96.98%)	(-97.55%)
	3	9	0	0.9	4.41	3.77	3.29	2.92	2.62
					(-98.49%)	(-98.71%)	(-98.87%)	(-99.00%)	(-99.10%)
	4	6	4	0.65	308.87	106.7	57.88	36.99	25.83
					(-65.46%)	(-81.26%)	(-88.02%)	(-91.64%)	
	4	6	4	0.77	30.44	16.67	11.17	8.24	6.44
					(-90.14%)	(-94.60%)	(-96.38%)	(-97.33%)	(-97.92%)
	4	6	4	0.9	3.65	3.07	2.65	2.34	2.08
					(-98.82%)	(-99.01%)	(-99.14%)	(-99.24%)	(-99.33%)

CUSUM exhibits approximately a 5% higher value than EWMA. Hence, when monitoring data from the INAR(1)DME process and accounting for various shift sizes, the CUSUM chart is the preferred choice for maintaining process control.

Table 11 ARL with deviation (in parenthesis) for the EWMA charts with $p_0 = 0.4$ and $\alpha_0 = -0.1$ having C chart with $u = (7,14)$

λ_0	q_0	θ	l	u	λ	α				
						-0.1	-0.3	-0.5	-0.7	-0.9
0.4	4	0.74	0	5	0.4	310.93	229.93	176.13	138.68	111.66
							(-26.05%)	(-43.35%)	(-55.40%)	(-64.09%)
	4	0.74	0	5	0.49	73.39	56.17	44.42	36.03	29.84
						(-76.40%)	(-81.93%)	(-85.71%)	(-88.41%)	(-90.40%)
	4	0.74	0	5	0.6	19.02	15.26	12.6	10.63	9.12
						(-93.88%)	(-95.09%)	(-95.95%)	(-96.58%)	(-97.07%)
	0	0.26	1	4	0.4	310.93	187.65	129.85	93.56	69.72
							(-34.29%)	(-54.53%)	(-67.24%)	(-75.58%)
	0	0.26	1	4	0.49	43.91	31.07	23.12	17.92	14.37
						(-84.62%)	(-89.12%)	(-91.90%)	(-93.72%)	(-94.97%)
	0	0.26	1	4	0.6	8.79	7	5.82	4.99	4.4
						(-96.92%)	(-97.55%)	(-97.96%)	(-98.25%)	(-98.46%)
	2	0.24	2	3	0.4	370.34	258.84	188.07	140.9	108.22
							(-30.11%)	(-49.22%)	(-61.95%)	(-70.78%)
	2	0.24	2	3	0.49	78.11	57.37	43.81	34.51	27.89
						(-78.91%)	(-84.51%)	(-88.17%)	(-90.68%)	(-92.47%)
	2	0.24	2	3	0.6	19.59	15.55	12.75	10.72	9.2
						(-94.71%)	(-95.80%)	(-96.56%)	(-97.11%)	(-97.52%)
0.65	5	0.13	3	6	0.65	298.78	172.68	107.23	70.71	49.07
							(-42.20%)	(-64.11%)	(-76.33%)	(-83.58%)
	5	0.13	3	6	0.77	17.71	13.31	10.48	8.55	7.17
						(-94.07%)	(-95.55%)	(-96.49%)	(-97.14%)	(-97.60%)
	5	0.13	3	6	0.9	3.21	2.85	2.56	2.33	2.13
						(-98.93%)	(-99.05%)	(-99.14%)	(-99.22%)	(-99.29%)
	6	0.32	1	8	0.65	299.98	192.51	130.51	92.44	67.87
							(-35.83%)	(-56.49%)	(-69.18%)	(-77.38%)
	6	0.32	1	8	0.77	19.5	14.77	11.63	9.45	7.87
						(-93.50%)	(-95.08%)	(-96.12%)	(-96.85%)	(-97.38%)
	6	0.32	1	8	0.9	3.06	2.69	2.4	2.17	1.97
						(-98.98%)	(-99.10%)	(-99.20%)	(-99.28%)	(-99.34%)
	9	0.53	0	10	0.65	301.39	208.18	150.09	111.93	85.83
							(-30.93%)	(-50.20%)	(-62.86%)	(-71.52%)
	9	0.53	0	10	0.77	21.19	16.28	12.93	10.56	8.8
						(-92.97%)	(-94.60%)	(-95.71%)	(-96.50%)	(-97.08%)
	9	0.53	0	10	0.9	2.99	2.61	2.32	2.08	1.88
						(-99.01%)	(-99.13%)	(-99.23%)	(-99.31%)	(-99.38%)

Table 12 ARL with deviation (in parenthesis) for the EWMA charts with $p_0 = 0.4$ and $\alpha_0 = 0.9$ having C chart with $u = (4, 8)$

λ_0	q_0	θ	l	u	λ	α				
						0.9	0.7	0.5	0.3	0.1
0.4	1	0.87	0	3	0.4	310.2	114.43	65.11	43.51	31.73
							(− 63.11%)	(− 79.01%)	(− 85.97%)	(− 89.77%)
	1	0.87	0	3	0.49	95.16	43.29	26.95	19.1	14.56
							(− 69.32%)	(− 86.04%)	(− 91.31%)	(− 93.84%)	(− 95.31%)
	1	0.87	0	3	0.6	27.38	16.03	11.2	8.54	6.86
							(− 91.17%)	(− 94.83%)	(− 96.39%)	(− 97.25%)	(− 97.79%)
	0	0.62	0	2	0.4	176.65	73.61	43.51	29.66	21.9
							(− 58.33%)	(− 75.37%)	(− 83.21%)	(− 87.60%)
	0	0.62	0	2	0.49	59.8	30.58	19.94	14.52	11.28
							(− 66.15%)	(− 82.69%)	(− 88.71%)	(− 91.78%)	(− 93.61%)
	0	0.62	0	2	0.6	19.66	12.6	9.22	7.25	5.95
							(− 88.87%)	(− 92.87%)	(− 94.78%)	(− 95.90%)	(− 96.63%)
0.65	6	0.81	0	7	0.65	303.9	109.36	62.14	41.51	30.22
							(− 64.01%)	(− 79.55%)	(− 86.34%)	(− 90.06%)
	6	0.81	0	7	0.77	34.74	18.93	12.78	9.54	7.55
							(− 88.57%)	(− 93.77%)	(− 95.79%)	(− 96.86%)	(− 97.52%)
	6	0.81	0	7	0.9	4.18	3.47	2.96	2.58	2.28
							(− 98.62%)	(− 98.86%)	(− 99.03%)	(− 99.15%)	(− 99.25%)
	2	0.64	0	6	0.65	300.19	106.53	59.2	38.81	27.84
							(− 64.51%)	(− 80.28%)	(− 87.07%)	(− 90.73%)
	2	0.64	0	6	0.77	32.31	18.08	12.36	9.3	7.41
							(− 89.24%)	(− 93.98%)	(− 95.88%)	(− 96.90%)	(− 97.53%)
	2	0.64	0	6	0.9	4.26	3.57	3.08	2.7	2.41
							(− 98.58%)	(− 98.81%)	(− 98.97%)	(− 99.10%)	(− 99.20%)
	3	0.29	1	4	0.65	322	107.61	56.04	34.82	23.92
							(− 66.58%)	(− 82.60%)	(− 89.19%)	(− 92.57%)
	3	0.29	1	4	0.77	28.34	16.13	11.01	8.25	6.54
							(− 91.20%)	(− 94.99%)	(− 96.58%)	(− 97.44%)	(− 97.97%)
	3	0.29	1	4	0.9	3.86	3.28	2.85	2.52	2.26
							(− 98.80%)	(− 98.98%)	(− 99.11%)	(− 99.22%)	(− 99.30%)

7.5 Real data analysis

The applicability of the CUSUM control chart is demonstrated by utilizing the disorderly conduct data set obtained from the 44th police car beat in Pittsburgh, (http://www.forecastingprinciples.com) which was used to fit the INAR(1)KF process introduced by Kim and Lee (2017), comprising of monthly observations from 1990 to 2001. It was used to monitor the mean under the INAR(1)KF process by Kim and Lee (2017). Initially, the data from 1990 to 1996 is used to fit the INAR(1)DME

Table 13 ARL of CUSUM and EWMA charts

α		$\lambda_0 = 0.4$		$\lambda_0 = 0.65$	
		CUSUM $k=2, h=10, c_0=4$	EWMA $q_0=0, \theta=0.26, l=1, u=4$	CUSUM $k=5, h=20, c_0=0$	EWMA $q_0=6, \theta=0.32, l=1, u=8$
	$\alpha_0 = -0.1$				
−0.1		300.25	310.93	288.72	299.98
−0.3		**184.7** (**−38.48%**)	187.65 (−34.29%)	**174.69** (**−39.50%**)	192.51 (−35.83%)
−0.5		**119.6** (**−60.17%**)	129.85 (−54.53%)	**111.65** (**−61.33%**)	130.51 (−56.49%)
−0.7		**80.89** (**−73.06%**)	93.56 (−67.24%)	**74.87** (**−74.07%**)	92.44 (−69.18%)
−0.9		**56.85** (**−81.07%**)	69.72 (−75.58%)	**52.46** (**−81.83%**)	67.87 (−77.38%)
	$\alpha_0 = 0.9$				
		CUSUM $k=1, h=5, c_0=4$	EWMA $q_0=1, \theta=0.87, l=0, u=3$	CUSUM $k=3, h=9, c_0=0$	EWMA $q_0=2, \theta=0.64, l=0, u=6$
0.9		297.06	310.2	292.12	300.19
0.7		**98.92** (**−66.70%**)	114.43 (−63.11%)	**99.56** (**−65.92%**)	106.53 (−64.51%)
0.5		**50.15** (**−83.12%**)	65.11 (−79.01%)	**53.06** (**−81.84%**)	59.2 (−80.28%)
0.3		**30.23** (**−89.82%**)	43.51 (−85.97%)	**33.69** (**−88.47%**)	38.81 (−87.07%)
0.1		**20.17** (**−93.21%**)	31.73 (−89.77%)	**23.63** (**−91.91%**)	27.84 (−90.73%)

Fig. 9 The time series plot of the disorderly conduct data set

process. Subsequently, the CUSUM control chart is applied to the data from 1997 to detect the presence of any significant mean increase.

Figure 9 displays the time series plot of the disorderly conduct data set (the dashed line denotes December 1996). Based on the plot, detecting the mean shift after the dashed line is challenging. For the data from 1990 to 1996 (phase I
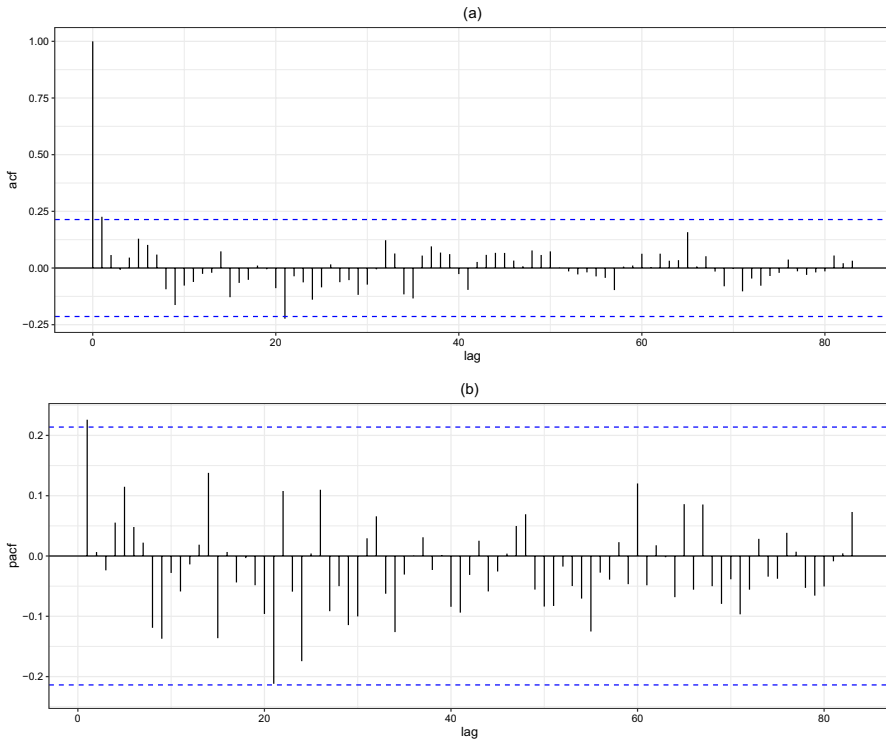
Fig. 10 The ACF (**a**) and PACF (**b**) plot of the phase I data set

Table 14 The CMLEs, logL, AIC, BIC and RMSE* of the considered processes for the phase I data set

Model	Parameters	CMLE	logL	AIC	BIC	RMSE*
INAR(1)DME	p	0.3789	− 174.874	355.747	363.040	2.270
	α	− 0.9999				
	λ	0.5957				
INAR(1)G	π	0.32	− 183.025	370.05	374.91	2.215
	α	0.50				
NBINARG(1)	μ	4.31	− 192.195	388.39	393.25	2.497
	α	0.80				
INARG(1)	p	0.26	− 196.05	396.1	400.96	2.264
	ρ	0.52				
INARP(1)	λ	3.13	− 181.365	366.73	371.59	2.12
	α	0.22				
INARNB(1)	n	11.64	− 179.33	364.66	371.95	2.123
	p	0.74				
	ρ	0.28				
QINARGP(1)	λ	3.51	− 179.815	365.63	372.93	2.121
	θ	0.13				
	ρ	0.26				
RCINARNB(1)	n	13.32	− 179.845	365.69	372.98	2.121
	p	0.77				
	ρ	0.26				
IINARNB(1)	n	5.20	− 259.255	524.51	531.8	6.154
	α	0.54				
	ρ	2.3×10^{-6}				
DCINARG(1)	μ	3.06	− 195.435	396.87	404.16	2.256
	α	0.53				
	θ	0.30				
INAR(1)ZP	λ	3.19	− 181.15	368.3	375.59	2.122
	ρ	0.6×10^{-7}				
	α	0.21				
INAR(1)KF	θ_1	2.21	− 179.145	364.29	371.58	2.119
	θ_2	0.25				
	α	0.25				

data), the sample mean and variance are obtained as 3.9643 and 5.3602, respectively. Figure 10 displays the ACF and PACF plots for the phase I data. Here, only the first lag is significant in the PACF plot, and the ACF plot displays an exponential decay, facilitating to model the data as an INAR(1) process. Hence, the data is modeled using the INAR(1)DME model and other competing models on the phase I data.
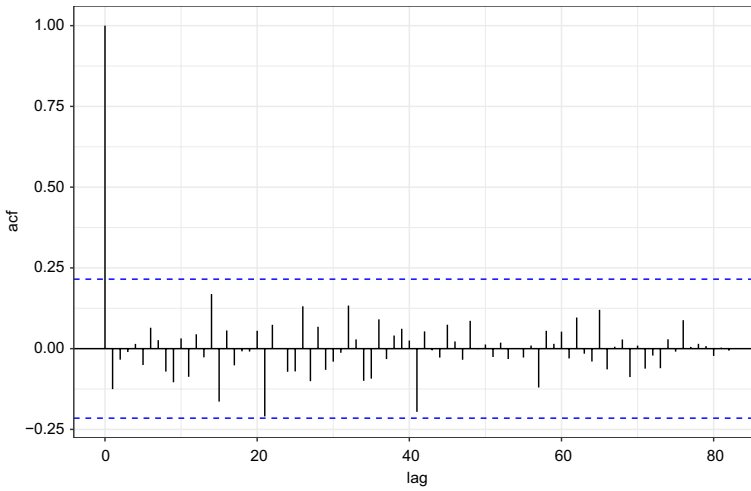
Fig. 11 The ACF plot of the Pearson residuals of the phase I data set

Table 15 ARL values of CUSUM chart for disorderly conduct data with $k = 4$ under the considered models

h	34	35	36	37	38	39	40	41	42
INAR(1)DME	161.7	170.5	179.6	188.9	198.0	208.65	218.98	229.64	240.62
INAR(1)KF	205.4	217.1	229.1	241.5	254.3	267.5	281	295	309
INARP(1)	235.1	248	261.1	274.7	288.6	302.8	317.4	332.3	347.6
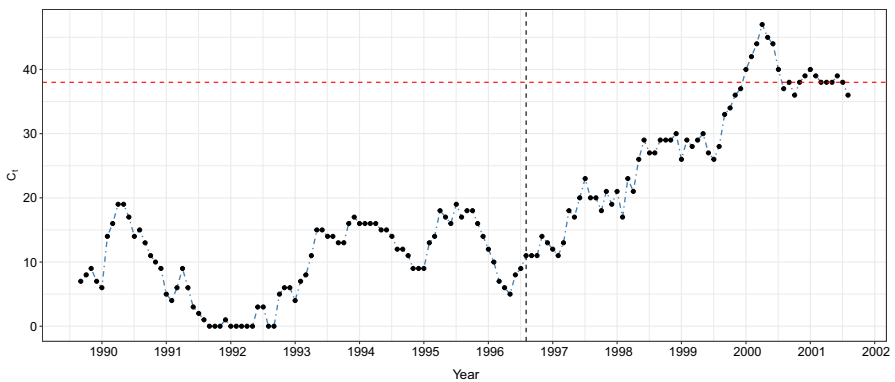
Fig. 12 The CUSUM plot of the monthly counts of disorderly conduct data

Table 14 lists the CMLEs, logL, AIC, BIC, and RMSE* for different processes. The maximum logL and minimum AIC and BIC values for the INAR(1)DME process show that it fits better than the contending models.

To check whether the fitted INAR(1)DME process is statistically accurate, residual analysis is done with the Pearson residuals. The ACF of the Pearson residuals is displayed in Fig. 11, showing no autocorrelation for the Pearson residuals. To ensure this, the Ljung-Box test for the presence of autocorrelation is done with degrees of freedom 10 and has the p-value $= 0.957 > 0.05$. It indicates that they are uncorrelated. Also, the mean and variance of Pearson residuals are 0.00228 and 0.83, close to the preferred values of 0 and 1, respectively, validating a good fit. Hence, the INAR(1)DME process fits the phase I data well.

The INAR(1)DME model for the phase I data is given by,

$$X_t = 0.3789 \circ X_{t-1} + \epsilon_t, \ t \geq 2, \tag{7.5}$$

where $\epsilon_t \sim \text{DME}(-0.9999, 0.5957)$.

The predicted values can be obtained by,

$$\hat{x}_1 = 3.8585,$$
$$\hat{x}_t = 0.3789 \, \hat{x}_{t-1} + 2.3963, \ t = 2, 3, \dots, 84.$$

Now, the CUSUM chart with reference value $k = 4$ (Kim and Lee 2017) is considered based on the INAR(1)DME process with parameters ($p = 0.3789, \ \alpha = -0.9999, \ \lambda = 0.5957$) and a suitable limit value h is chosen.

Table 15 provides the ARL values of CUSUM chart with respect to INAR(1) DME, INAR(1)KF and INARP(1) processes for $k = 4$ and $c_0 = 0$, respectively. Here, the ARL values with respect to the INAR(1)DME process are lower than those of the INAR(1)KF and INARP(1) processes. The lower ARL values indicate quicker identification of process deviation, leading to the conclusion that the CUSUM chart based on the INAR(1)DME process outperforms the others. Taking $ARL_0 = 200$, the upper control limit CUSUM chart under the INAR(1)DME process is obtained as $h = 38$.

The CUSUM chart for disorderly conduct data under INAR(1)DME process is given in Fig. 12, where the red horizontal dashed and vertical dashed lines respectively stand for $h = 38$ and December 1996.

From the plot, it is clearly seen that $C_t \geq h$ occurred in May 2000. The sample mean of the data from January 1997 to May 2000 is 4.7073, which is greater than that of the past observations. Identifying this phenomenon is challenging unless the CUSUM control scheme has been implemented.

8 Conclusion

This paper presents a novel discrete analog of the mixture exponential distribution, namely the DME distribution, by utilizing the survival discretization technique. The statistical properties of the DME distribution are discussed, and the simulation study suggests that ML estimation outperforms LS methods. The performance of the DME

distribution in modeling real data enables further exploration of its application in the field of time series. Consequently, an associated INAR(1) process with DME innovations is introduced, accompanied by a comprehensive investigation into its statistical characteristics and performance through extensive simulation studies. The work also extends to the domain of process monitoring, where custom control charts are developed to track the process mean. In this context, CUSUM and EWMA control charts are developed to monitor the mean of the INAR(1)DME process, and their effectiveness in detecting shifts is meticulously analyzed, providing valuable insights through comparative assessments. Additionally, the practical applicability of the INAR(1)DME process is confirmed through its use with real-world data under the CUSUM chart, showcasing its relevance in both statistical theory and real-world process monitoring and control applications.

Appendix: Moments

The mean of the DME distribution is obtained as,

$$
\begin{aligned}
\mu'_1 &= \sum_{x=0}^{\infty} x\{\lambda^x(1-\lambda)(1-\alpha) + \alpha\lambda^{2x}(1-\lambda^2)\} \\
&= \frac{\lambda(1-\lambda)(1-\alpha)}{(1-\lambda)^2} + \frac{\alpha(1-\lambda^2)\lambda^2}{(1-\lambda^2)^2} \\
&= \frac{(1-\alpha+\lambda)\lambda}{(1-\lambda^2)}.
\end{aligned}
$$

The rest of the moments are given by,

$$
\mu'_2 = \frac{\lambda((1+\lambda)^3 - \alpha(1+2\lambda+3\lambda^2))}{(1-\lambda^2)^2},
$$

$$
\mu'_3 = \frac{\lambda((1+\lambda)^3(1+4\lambda+\lambda^2) - \alpha(1+6\lambda+16\lambda^2+12\lambda^3+7\lambda^4))}{(1-\lambda^2)^3},
$$

$$
\mu'_4 = \frac{\lambda((1+\lambda)^5(1+10\lambda+\lambda^2) - \alpha(1+14\lambda+61\lambda^2+104\lambda^3+115\lambda^4+50\lambda^5+15\lambda^6))}{(1-\lambda^2)^4}.
$$

Then, the central moments are obtained as,

$$
\mu_2 = \frac{\lambda((1+\lambda)^2 - \alpha^2\lambda - \alpha(1+\lambda^2))}{(1-\lambda^2)^2},
$$

$$
\mu_3 = \frac{\lambda((1+\lambda)^3(1+3\lambda-4\lambda^2) - \alpha^2\lambda(1+6\lambda+11\lambda^2) - \alpha(1+4\lambda+2\lambda^2-16\lambda^3-9\lambda^4))}{(1-\lambda^2)^3},
$$

$$
\begin{aligned}
\mu_4 &= \frac{\lambda((1+\lambda)^4(1+7\lambda+\lambda^2) - 3\alpha^4\lambda^3 - 6\alpha^3(\lambda^2+\lambda^4) - 2\alpha^2\lambda(2+3\lambda+14\lambda^2+3\lambda^3+2\lambda^4))}{(1-\lambda^2)^4} \\
&\quad - \frac{\lambda(\alpha(1+6\lambda+23\lambda^2+12\lambda^3+23\lambda^4+6\lambda^5+\lambda^6))}{(1-\lambda^2)^4}.
\end{aligned}
$$

References

Ahsan-ul Haq M, Irshad MR, Muhammed Ahammed ES, Maya R (2023) New discrete Bilal distribution and associated INAR(1) process. Lobachevskii J Math 44(9):3647–3662

Al-Osh MA, Aly E-EA (1992) First order autoregressive time series with negative binomial and geometric marginals. Commun Stat Theory Methods 21(9):2483–2492

Al-Osh MA, Alzaid AA (1987) First-order integer-valued autoregressive (INAR(1)) process. J Time Ser Anal 8(3):261–275

Altun E, Khan NM (2022) Modelling with the novel INAR(1)-PTE process. Methodol Comput Appl Probab 24:1735–1751

Altun E, El-Morshedy M, Eliwa MS (2022) A study on discrete Bilal distribution with properties and applications on integer valued autoregressive process. REVSTAT Stat J 20(4):501–528

Alzaid A, Al-Osh M (1988) First-order integer-valued autoregressive (INAR(1)) process: distributional and regression properties. Stat Neerl 42(1):53–61

Alzaid AA, Al-Osh MA (1993) Some autoregressive moving average processes with generalized Poisson marginal distributions. Ann Inst Stat Math 45:223–232

Bodhisuwan W, Sangpoom S (2016) The discrete weighted Lindley distribution. In: 2016 12th International Conference on Mathematics, Statistics, and Their Applications (ICMSA). IEEE, pp 99–103

Chakraborty S, Chakravarty D (2014) A discrete Gumbel distribution. arXiv preprint arXiv:1410.7568

El-Morshedy M, Eliwa MS, Altun E (2020) Discrete Burr–Hatke distribution with properties, estimation methods and regression model. IEEE Access 8:74359–74370

Harvey AC, Fernandes C (1989) Time series models for count or qualitative observations. J Bus Econ Stat 7(4):407–417

Jazi MA, Jones G, Lai C-D (2012) Integer valued AR (1) with geometric innovations. J Iran Stat Soc 11(2):173–190

Jazi MA, Jones G, Lai C-D (2012) First-order integer valued AR processes with zero inflated Poisson innovations. J Time Ser Anal 33(6):954–963

Kim H, Lee S (2017) On first-order integer-valued autoregressive process with Katz family innovations. J Stat Comput Simul 87(3):546–562

Krishna H, Pundir PS (2009) Discrete Burr and discrete Pareto distributions. Stat Methodol 6(2):177–188

Li C, Wang D, Zhu F (2016) Effective control charts for monitoring the NGINAR (1) process. Qual Reliab Eng Int 32(3):877–888

Li C, Wang D, Zhu F (2019) Detecting mean increases in zero truncated INAR (1) processes. Int J Prod Res 57(17):5589–5603

Li C, Zhang H, Wang D (2022) Modelling and monitoring of INAR(1) process with geometrically inflated Poisson innovations. J Appl Stat 49(7):1821–1847

Maya R, Chesneau C, Krishna A, Irshad MR (2022) Poisson extended exponential distribution with associated INAR(1) process and applications. Stats 5(3):755–772

McKenzie E (1986) Autoregressive moving-average processes with negative-binomial and geometric marginal distributions. Adv Appl Probab 18(3):679–705

Mirhossaini SM, Dolati A (2008) On a new generalization of the exponential distribution. J Math Ext 3:27–42

Page E (1961) Cumulative sum charts. Technometrics 3(1):1–9

Para BA, Jan TR (2016) Discrete version of log-logistic distribution and its applications in genetics. Int J Mod Math Sci 14(4):407–422

Rakitzis AC, Weiß CH, Castagliola P (2017) Control charts for monitoring correlated Poisson counts with an excessive number of zeros. Qual Reliab Eng Int 33(2):413–430

Ristić MM, Bakouch HS, Nastić AS (2009) A new geometric first-order integer-valued autoregressive (NGINAR(1)) process. J Stat Plan Inference 139(7):2218–2226

Ristić MM, Nastić AS, Miletić Ilić AV (2013) A geometric time series model with dependent Bernoulli counting series. J Time Ser Anal 34(4):466–476

Roberts S (2000) Control chart tests based on geometric moving averages. Technometrics 42(1):97–101

Roy D (2004) Discrete Rayleigh distribution. IEEE Trans Reliab 53(2):255–260

Weiß CH (2008) Thinning operations for modeling time series of counts: a survey. AStA Adv Stat Anal 92:319–341

Weiß CH (2009) EWMA monitoring of correlated processes of Poisson counts. Qual Technol Quant Manag 6(2):137–153

Weiß CH (2011) Detecting mean increases in Poisson INAR (1) processes with EWMA control charts. J Appl Stat 38(2):383–398

Weiß CH (2018) An introduction to discrete-valued time series. Wiley, New York

Weiß CH, Testik MC (2009) CUSUM monitoring of first-order integer-valued autoregressive processes of Poisson counts. J Qual Technol 41(4):389–400

Weiß CH, Testik MC (2011) The Poisson INAR (1) CUSUM chart under overdispersion and estimation error. IIE Trans 43(11):805–818

Zhang M, Nie G, He Z, Hou X (2014) The Poisson INAR (1) one-sided EWMA chart with estimated parameters. Int J Prod Res 52(18):5415–5431